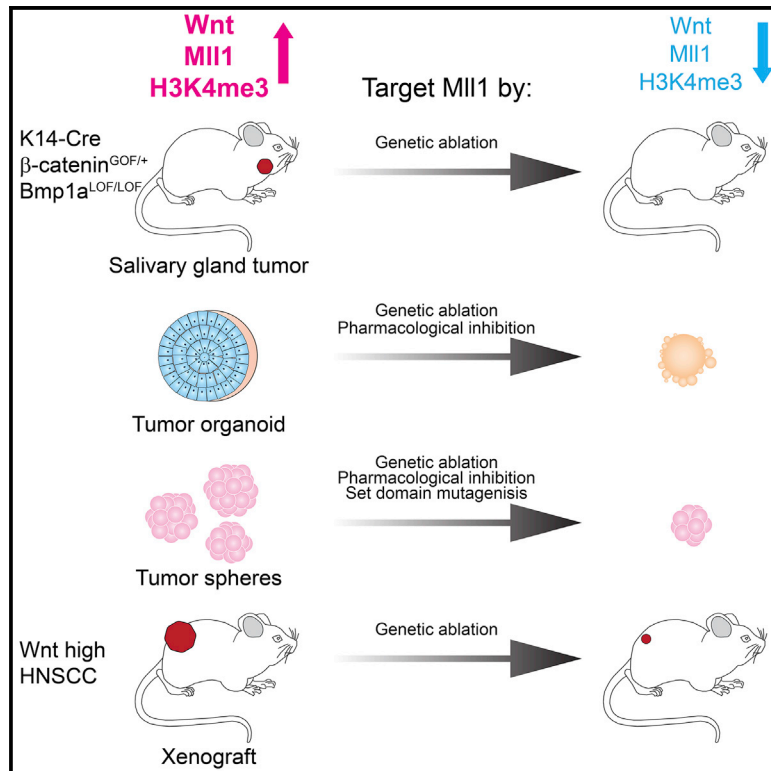# The Wnt-Driven Mll1 Epigenome Regulates Salivary Gland and Head and Neck Cancer

Graphical Abstract

Authors

Qionghua Zhu, Liang Fang,
Julian Heuberger, ...,
Annika Wulf-Goldenberg, Sascha Sauer,
Walter Birchmeier

Correspondence

wbirch@mdc-berlin.de

In Brief

Mutations of *Mll1* genes were described in leukemia, but little is known about the roles of *Mll1* in solid tumors. Zhu et al. provide genetic evidence for a crucial role of Mll1 in Wnt/β-catenin-driven salivary gland and head and neck cancers.

Highlights

- High Wnt/β-catenin and Mll1 are linked to high H3K4me3 at promoters in mouse tumors

- Mll1 is required for the initiation and maintenance of salivary gland tumors

- SET domain mutations of Mll1 reduce the self-renewal of tumor-propagating cells

- Genetic Mll1 ablation reduces tumor initiation of human head and neck cancer cells

CellPress

The Wnt-Driven Mll1 Epigenome Regulates Salivary Gland and Head and Neck Cancer

Qionghua Zhu,[1,8] Liang Fang,[1,2,3,8] Julian Heuberger,[1] Andrea Kranz,[4] Jörg Schipper,[5] Kathrin Scheckenbach,[5] Ramon Oliveira Vidal,[6] Daniele Yumi Sunaga-Franze,[6] Marion Müller,[1] Annika Wulf-Goldenberg,[7] Sascha Sauer,[6] and Walter Birchmeier[1,9,*]

[1]Cancer Research Program, Max Delbrück Center for Molecular Medicine (MDC) in the Helmholtz Society, 13125 Berlin, Germany
[2]Department of Biology, Southern University of Science and Technology (SUSTech), Shenzhen 518055, China
[3]Medi-X Institute, SUSTech Academy for Advanced Interdisciplinary Studies, Southern University of Science and Technology (SUSTech), Shenzhen 518055, China
[4]Biotechnology Center, Technical University, 01307 Dresden, Germany
[5]Department of Head and Neck Surgery, Heinrich Heine University, 40225 Düsseldorf, Germany
[6]Systems Biology Program, Max Delbrück Center for Molecular Medicine (MDC) in the Helmholtz Society, 13125 Berlin, Germany
[7]Experimental Pharmacology & Oncology (EPO), 13125 Berlin, Germany
[8]These authors contributed equally
[9]Lead Contact
*Correspondence: wbirch@mdc-berlin.de
https://doi.org/10.1016/j.celrep.2018.12.059

SUMMARY

We identified a regulatory system that acts downstream of Wnt/β-catenin signaling in salivary gland and head and neck carcinomas. We show in a mouse tumor model of K14-Cre-induced *Wnt/β-catenin* gain-of-function and *Bmpr1a* loss-of-function mutations that tumor-propagating cells exhibit increased Mll1 activity and genome-wide increased H3K4 trimethylation at promoters. Null mutations of *Mll1* in tumor mice and in xenotransplanted human head and neck tumors resulted in loss of self-renewal of tumor-propagating cells and in block of tumor formation but did not alter normal tissue homeostasis. CRISPR/Cas9 mutagenesis and pharmacological interference of Mll1 at sequences that inhibit essential protein-protein interactions or the SET enzyme active site also blocked the self-renewal of mouse and human tumor-propagating cells. Our work provides strong genetic evidence for a crucial role of Mll1 in solid tumors. Moreover, inhibitors targeting specific Mll1 interactions might offer additional directions for therapies to treat these aggressive tumors.

INTRODUCTION

Head and neck cancers comprise a heterogeneous group of tumors that arise in the paranasal sinus, oral and nasal cavities, pharynx and larynx, and salivary glands. 90% of these tumors are squamous cell carcinomas and are newly diagnosed in 600,000 patients annually. Only 40%–50% will survive 5 years, making this the fifth-most frequent malignant cancer worldwide (Leemans et al., 2011; Morris et al., 2017). The most important risk factors for head and neck squamous cell carcinomas (HNSCCs) are smoking, excess alcohol consumption, and infection by high-risk human papillomaviruses (HPVs). Molecular therapies to treat advanced, recurrent, or metastatic HNSCCs are lacking; radio- and chemotherapies and EGFR antibody therapies using cetuximab have limited success and are often accompanied by impairing side effects (Bauml et al., 2016; Jäckel and Scheckenbach, 2014; Matuschek et al., 2016). Salivary gland squamous cell carcinomas (SG-SCCs) are also difficult to treat, because they are aggressive and produce early lymphatic metastases (Konings et al., 2006; Ying et al., 2006).

Next-generation sequencing of HNSCCs has revealed inactivating mutations of *TP53*, *NOTCH1*, *NSD1*, *CDKN2A*, *FBXW7*, *CASP8*, and *PTEN* and activating mutations of *PIK3CA*, *HRAS*, and others (Alioto et al., 2015; Cancer Genome Atlas Network, 2015; Hoesli et al., 2017; Mountzios et al., 2014). HNSCC tumors also exhibit activation of Wnt/β-catenin signaling, and mutations have been found in the Wnt pathway components *AJUBA*, *FRZR*, *DKK3*, and *FAT1* (Cancer Genome Atlas Network, 2015; Díaz Prado et al., 2009; Katase et al., 2012). *NOTCH*, *FAT1*, and *AJUBA*, three genes that can influence Wnt signaling via the inhibition of β-catenin, are frequently altered in HPV⁻ carcinomas (Cancer Genome Atlas Network, 2015; Haraguchi et al., 2008; Kwon et al., 2011; Morris et al., 2013). A large consortium has reported common molecular features of various human squamous cell carcinomas from five sites, from head and neck to bladder cancer, which correlated with DNA mutations and methylations, microRNA expression, squamous cell stemness, epithelial-to-mesenchymal differentiation, oxidative damage, and other features. These findings support possibilities for common therapeutic approaches for the different squamous cell carcinomas (Campbell et al., 2018).

We showed in a previous report (Wend et al., 2013) that mice harboring *β-catenin* gain-of-function (GOF) and *Bmpr1a* loss-of-function (LOF) mutations driven by *K14-Cre* develop salivary gland squamous cell carcinomas within 100 days after birth.

Aggressive tumors appeared rapidly in the salivary glands of the double mutants. The tumors were classified as salivary gland squamous cell carcinomas by histopathological criteria, contained keratin pearls, and expressed high levels of the tumor marker K10 (Chu and Weiss, 2002). These pieces of evidence support the notion that Wnt/β-catenin signaling plays a significant role in the progression of salivary gland tumors and in the survival of mice.

Tumors contain tumor-propagating cells that have been linked to therapy resistance and are increasingly considered prime targets for novel treatment strategies. Studies suggest that Wnt/β-catenin signaling controls tumor-propagating cells in HNSCCs. The Wnt antagonist sFRP4 reduced β-catenin expression and suppressed the stem cell markers CD44 and ALDH, changes that were accompanied by reduced proliferation (Warrier et al., 2014). Tumor-propagating cells also appear to play key roles in the metastatic potential and the frequency of relapse of HNSCCs (Prince et al., 2007; Zhang et al., 2012). We had shown in our previous report (Wend et al., 2013) that more than 90% of the mouse salivary gland CD24+DC29+SEEA1+ tumor-propagating cells exhibited nuclear β-catenin and were low in Smad 1/5/8 compared to unsorted cells.

Histone methyltransferases such as mixed-lineage leukemia (Mll) 1 help configure the chromatin environment as central mechanisms of gene regulation, but it has not been clear how the activity of Mll1 is regulated in solid cancer, and how it may interact with Wnt/β-catenin signaling. Our previous study showed that β-catenin, CBP, and Mll1 are critical for the tumor growth and stem cell maintenance *in vitro* and with xenografts, and they may be involved in a transcription complex that promotes histone H3 lysine 4 (H3K4) tri-methylation in the tumor-propagating population (Wend et al., 2013). Here we investigated the role of Mll1 in tumor initiation genetically, demonstrated that the interaction between Mll1 and β-catenin is essential for their functions, and defined the role of H3K4 methyltransferase activity in the transcriptional response to Wnt/β-catenin signals in salivary gland squamous cell cancer in mice. We also demonstrated similar mechanisms in human head and neck squamous cell carcinoma cell lines.

RESULTS

Mouse Salivary Gland Tumor-Propagating Cells Display an Epigenome Profile of H3K4 Hypermethylation

Mice harboring β-catenin gain-of-function (β-catenin^f/+) and Bmpr1a loss-of-function (Bmpr^f/f) mutations driven by Keratin (K) 14-Cre develop salivary gland squamous cell carcinomas within 100 days after birth (Figures S1A and S1B) (Wend et al., 2013). The tumors were classified as SG-SCCs by histopathological criteria. Consistent with human tumors, mouse SG-SCCs also showed high Wnt and low Bmp signals. In these tumors, it is possible to distinguish a subpopulation endowed with enhanced tumorigenic potential—referred to as tumor-propagating cells—through the presence of nuclear β-catenin, a hallmark of strong Wnt signaling; another distinguishing feature is the expression of K14 (Figure S1C, with tumor-propagating cells marked by white arrowheads). By fluorescence-activated cell sorting (FACS), tumor-propagating cells were enriched

from salivary gland tumors as CD24^high CD29^high cells and then cultured as large spheres in non-adhesive conditions, which rapidly propagated (Figures S1D and S1E). Spheres had increased expression of stem cell-associated genes and Wnt/β-catenin target genes, in contrast to adherent cells (Figure S1F). Western blots of histone extracts showed enhanced modification of H3K4 tri-methylation (H3K4me3) in sphere culture (Figure S1G). We had shown in our previous report (Wend et al., 2013) that more than 90% of the mouse salivary gland CD24+DC29+ cells exhibited nuclear β-catenin and a low level of Smad 1/5/8 and were hyperproliferative and highly tumorigenic when 500 cells were transplanted into the back skin of non-obese diabetic-severe combined immunodeficiency (NOD-SCID) mice, confirming them as tumor-propagating cells. Unsorted cells were a little tumorigenic (100,000 cells were required).

Cancer cells from salivary gland tumors were kept in adherent (Ad) (differentiated cancer cell) or sphere (Sp) (tumor-propagating cell) culture and then subjected to chromatin immunoprecipitation sequencing (ChIP-seq) and mRNA sequencing (mRNA-seq) using antibodies specific for histone modifications: H3K4 monomethylation (H3K4me1), H3K4 dimethylation (H3K4me2), and H3K4me3. An assessment of normalized ChIP-seq read densities (in reads per million) in peak regions showed marked enrichment of levels of H3K4me1, H3K4me2, and H3K4me3 in sphere compared to adherent cultures (Figures 1A–1C). The two states exhibited significant differences in global peak enrichment and representation at transcriptional start sites (TSSs), as determined through statistical comparisons (Figures S1H and S1I). The main increases in H3K4me2 and H3K4me3, but not H3K4me1, were observed in Sp cultures in regions of gene promoters (Figure S1K, lower pictures, in blue), in which these marks typically have an activating role for transcription. Moreover, upregulated genes showed globally increased levels of H3K4me3 at promoter regions compared to downregulated genes (Figure S1J) (difference 9.6e−7). In Sp cultures, a high level of H3K4me3 was observed at the promoter region of Axin2, Id2, Tcf7l2, Tiam1, and Ephb3, well-characterized Wnt target genes (Lustig et al., 2002) that are expressed at high levels in Sp cultures, and was confirmed by RNA sequencing (RNA-seq) (Figure 1D; Figures S2A–S2D). A similar pattern was observed for Olfm4, an intestinal stem cell marker (van der Flier et al., 2009), which is associated with Wnt activation (Figure 1E). We also performed immunofluorescence analyses of histone modifications on sections of salivary gland tumors: H3K4me3 levels were enriched in nests of β-catenin^high cells (Figures 1F, upper panel, merged fluorescence on the right, and 1G). In contrast, the polycomb-dependent repressive histone mark histone H3 lysine 27 tri-methylation (H3K27me3) was reduced in the nests of β-catenin^high tumor-propagating cells (Figures 1F, lower panel, and 1G). These results establish that active Wnt/β-catenin signaling and chromatin modifications are linked through H3K4 tri-methylation. To identify which groups of genes were mostly affected by H3K4me2 and H3K4me3, gene ontology analysis was performed; it revealed that genes involved in cytokine production pathway showed elevated levels of H3K4me2 and H3K4me3 modification and
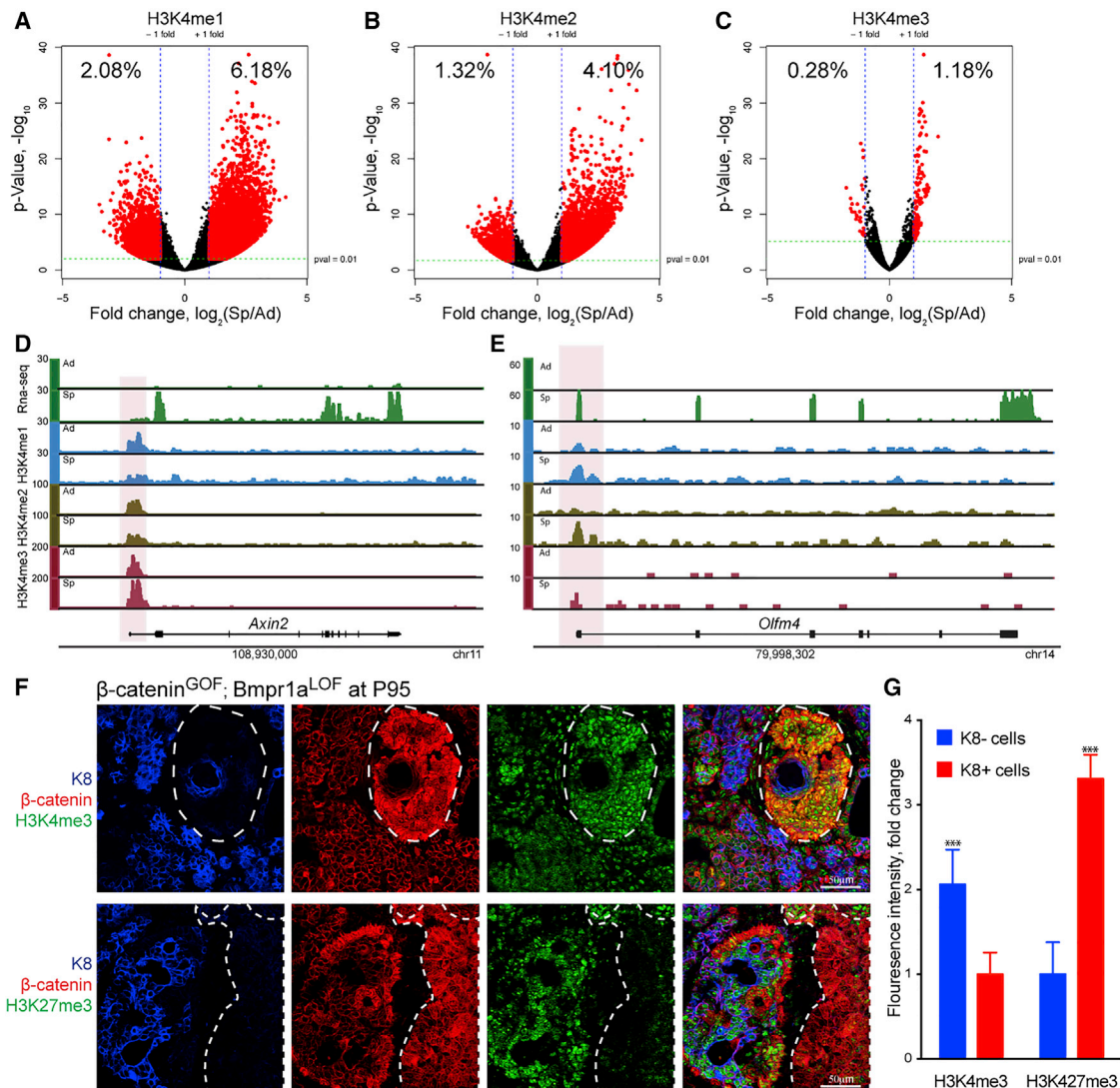
Figure 1. Histone Modifications in Salivary Gland Tumor Cells

(A–C) Comparison of global levels of H3K4me1 (A), H3K4me2 (B), and H3K4me3 (C) in tumor-propagating cells (sphere culture [Sp]) and differentiated cancer cells (adherent culture [Ad]) using ChIP-seq. Fold changes of histone modifications on peak regions are plotted against the p value. Significantly changed peak regions are marked in red. Values of three replicates were averaged.

(D and E) H3K4me changes in Ad and Sp cultures of Wnt/β-catenin target genes *Axin2* (D) and *Olfm4* (E). Promoter regions are marked horizontally.

(F) Immunofluorescence staining of cytokeratin 8 (blue), β-catenin (red), and histone H3 modifications (H3K4me3 and H3K27me3, green) on salivary gland tumor sections. Merging of colors is shown on the far right.

(G) Quantification of viable H3K4me3 and H3K27me3 in tumor-propagating and tumor cells. Error bars, mean ± SD. ***p < 0.001.

See also Figures S1 and S2.

mRNA expression in tumor-propagating cells (Figure S2H), including Il1a, Il23a, and Cxcr2 (Figures S2E–S2G). In addition, treatment with MI-2, which reduces the activity of Mll1 (Grembecka et al., 2012), downregulated the expression of these genes (Figure S2I).

Mll1 Is Associated with Wnt/β-Catenin Signaling in Salivary Gland Tumor-Propagating Cells

Mll methyltransferases produce methylated H3K4 in mammalian cells (Wang et al., 2009). We analyzed the expression levels of

the six *Mll* family members using quantitative real-time PCR in freshly isolated salivary gland tumor cells and in cells following adherent and sphere culture. Mutant β-catenin^{GOF}; Bmpr1a^{LOF} tumor cells (called double-mutant tumor cells) showed mildly reduced changes in the expression levels of the *Mll* family members compared to control and *β-catenin* single-mutant cells, and the levels were similar to the ones observed in double-mutant tumor cells propagated by adherent conditions (Figure S3A). However, in sphere cultures of double-mutant tumor cells, in which tumor-propagating cells are highly enriched (as described
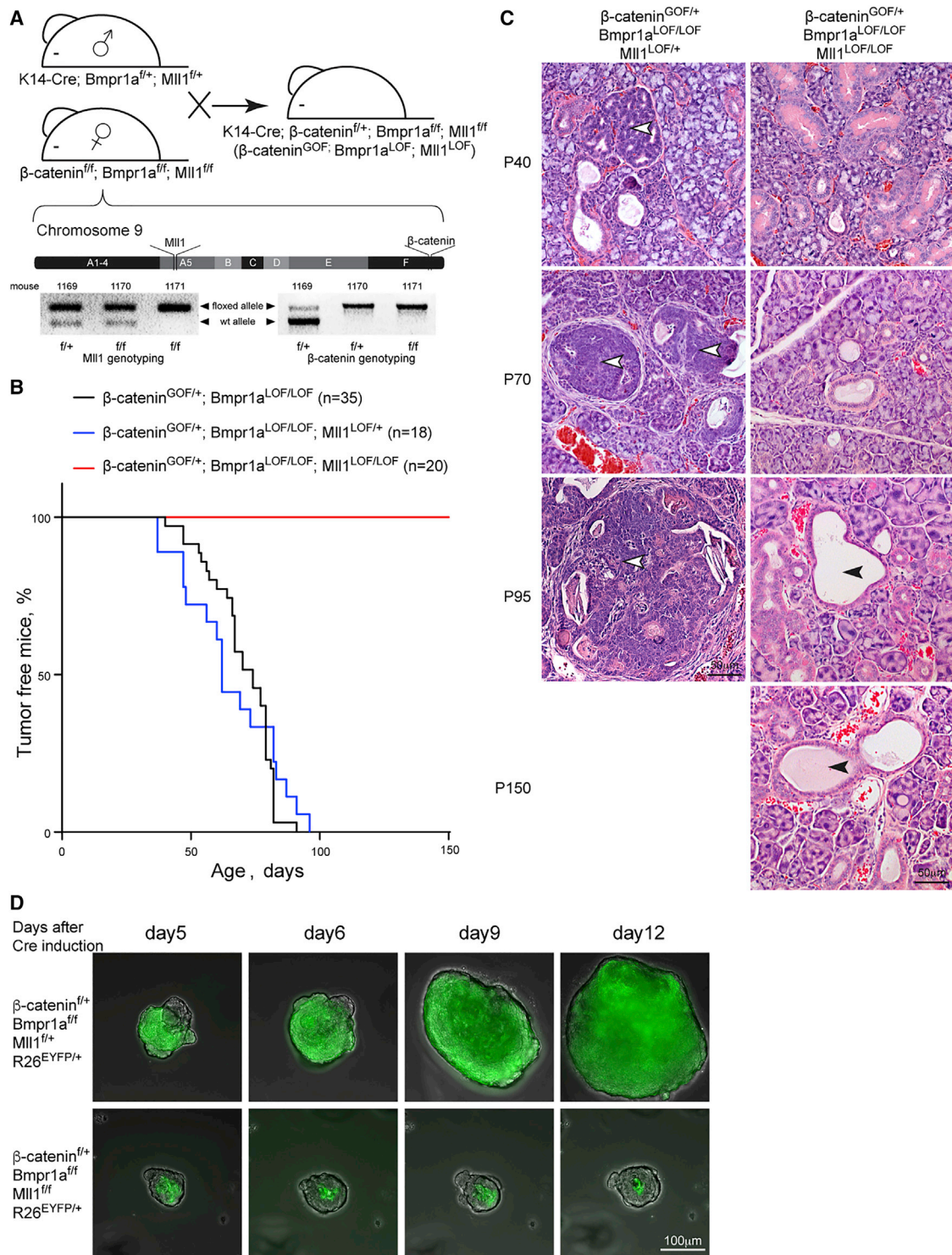
Figure 2. Homozygous Deletion of Mll1 Prevents Salivary Gland Tumor Formation

(A) Triple-mutant mice of the genotype *K14-Cre; β-catenin^f/+; Bmpr1a^f/f; Mll1^f/f* were generated. The generation of the *β-catenin* and *Mll1* double-floxed allele was confirmed by PCR genotyping (mouse 1171).

(B) Tumor-free survival curves are shown for mice with *β-catenin; Bmpr1a* double mutations (black curve, n = 35 mice), with *β-catenin; Bmpr1a* double mutations and heterozygous *Mll1* ablation (blue, n = 18 mice), and with *β-catenin; Bmpr1a* double mutations and homozygous *Mll1* ablation (red, n = 20 mice).

(legend continued on next page)

earlier), the expression levels of *Mll1* and *Mll3* were increased (Figure S3A, far right).

Two members of the Mll family, Mll1 and Setd1a, have been shown to interact in cell culture with the β-catenin transcription factor complex involved in Wnt target gene activation (Salz et al., 2014; Sierra et al., 2006). Because deletion of *Mll3* had no effect on tumor growth (as described later), and because the expression of Setd1a was not upregulated in the spheres (Figure S3A), we focused on Mll1. In cells, Mll1 binds indirectly to β-catenin via the Creb-binding protein (CBP), a histone acetyltransferase (scheme in Figure S3B) (Arai et al., 2010; Ernst et al., 2001; Takemaru and Moon, 2000). To test whether this interaction also occurs in mouse salivary gland tumor-propagating cells, β-catenin and the associated transcription factors LEF1 or TCF4 were immunoprecipitated from cells that were enriched in sphere culture and analyzed by western blot. Both Mll1 and CBP were detected in the immunoprecipitated β-catenin transcription factor complex, whose predominant component was TCF4 (Figure S3C). The formation of the complex was disrupted after incubation with the Wnt inhibitor ICG-001, which blocks β-catenin/CBP, and with LF3, which interferes with β-catenin/TCF4 (Emami et al., 2004; Fang et al., 2016): immunoprecipitation of Mll1 in the presence of ICG-001 showed reduced β-catenin and TCF4 levels, but compound LF3 reduced only TCF4 (Figure S3D).

We also examined whether Wnt/β-catenin signaling regulates the expression of *Mll1* in salivary gland tumor cells. Sequences upstream of the *Mll1* gene were examined using the Patch1.0 program of Genexplain. This revealed five potential TCF-LEF binding sites between positions −4 and −8 kb, which were clustered in two regions, called regions 1 and 2 (Figure S3E). To test whether these sites respond to Wnt activity, regions 1 and 2 were cloned into the luciferase reporter plasmid pGL4.23 and transfected into HEK293 cells. Upon stimulation of the Wnt pathway by the GSK3β inhibitor CHIR99021, which is a strong Wnt activator, both regions responded to treatment. However, region 2 was less sensitive to mild activation induced by Wnt3a (Figure S3F). These results show that β-catenin physically interacts with the Mll1 protein complex in salivary gland tumor cells and may contribute to the upregulated transcription of the *Mll1* gene.

Genetic Experiments Show that Mll1 Is Required for the Initiation of Mouse Salivary Gland Tumors

To genetically examine the role of *Mll1* in the generation of mouse salivary gland tumors, we generated triple-mutant mice with the genotype *K14-Cre; β-catenin^{f/+}; Bmpr1a^{f/f}; Mll1^{f/f}* (Figure 2A) (Kranz et al., 2010). The *β-catenin* and *Mll1* genes in mice are located on the same chromosome but at considerable distance; therefore, we could generate mice with a version of chromosome 9 that harbored both floxed *β-catenin* and floxed *Mll1* through chromosomal crossover during breeding, i.e., mouse 1171 (see PCR genotyping in Figure 2A). Thus, we finally

produced triple mutants, *Mll1^{LOF/+}* and *Mll1^{LOF/LOF}* mice on the tumor background (Figure 2B, upper part, crossings and numbers of offspring). All triple-mutant mice carrying a heterozygous deletion of *Mll1* developed tumors by post-natal day (P) 100; the initiation and progression of the tumors were similar to those of double-mutant mice (Figures 2B, lower part, compare blue and black curves, and 2C, carcinomas in the left column, marked by white arrowheads). In contrast, triple-mutant mice with homozygous deletion of *Mll1* did not produce tumors in the salivary glands, even at 150 days (Figures 2B, red curve, and 2C, right column). Only mild hyperplasia was observed at late time points, P95 and P150 (Figure 2C, right column, marked by black arrowheads).

We also examined the influence of *Mll1* ablation on initiation of salivary gland tumors in salivary gland organoid culture. Organoids were generated from *β-catenin^{f/+}; Bmpr1a^{f/f}; Mll1^{f/+}* and *β-catenin^{f/+}; Bmpr1a^{f/f}; Mll1^{f/f}* cells, and mutations were introduced by transduction with a retroviral construct producing Cre recombinase. Cells used to generate the organoids also contained the floxed *ROSA26^{EYFP/+}* reporter allele, which is activated by Cre. Cells with heterozygous ablation of *Mll1* grew rapidly and formed tumor-like organoids that were filled, unstructured, and highly proliferative (Figure 2D, upper panel; Figure S4A, upper panel). In contrast, organoids with homozygous ablation of *Mll1* displayed reduced proliferation and an increase in apoptosis (Figure 2D, lower panel; Figure S4A, lower panel).

During development, homozygous *Mll1* ablation driven by *K14-Cre* (*Mll1^{LOF}*) produced no changes in the overall morphology and histological appearance of the salivary glands (Figures S4B and S4C). *Mll1^{LOF}* mice had similar numbers of salivary gland ducts as control animals (Figure S4C, marked by white arrowheads), and the distribution of cells marked by EYFP was similar to that seen in control cells (Figure S4D, marked by a broken white line).

Mll1 Is Required for Tumor Maintenance in Mouse Salivary Gland Organoids

To examine whether *Mll1* is also required for tumor maintenance, we used the small molecule Mll1/Menin interaction inhibitor MI-2 that reduces the activity of Mll1 (Grembecka et al., 2012). Control and *β-catenin^{GOF}; Bmpr1a^{LOF}* (double mutant) cells were isolated from the salivary gland by FACS and then raised in 3D culture to generate organoids (Clevers, 2016; Maimets et al., 2016). In 4 days, control organoids built slow-growing lobular structures with basal and luminal cells, which showed K14 and K8 expression, respectively (Figures 3A, upper panel, and 3B, upper panel), while double-mutant cells generated fast-growing organoids that were filled and were composed of basal K14-expressing cells as observed *in vivo* (Figures 3A, lower panel, and 3B, second panel). The Mll1 inhibitor MI-2 did not significantly affect the growth of the control organoids (Figure 3B, third panel, quantified in

---

(C) Histological comparison between salivary gland tissues of double-mutant mice plus heterozygous and homozygous Mll1 ablation at different ages. White arrowheads on the left show tumor lesions; black arrowheads on the right show hyperplastic lesions.
(D) Time-dependent rapid growth of filled tumor-like organoids with heterozygous ablation of *Mll1* (upper row of pictures). Reduced growth of organoids with homozygous ablation of *Mll1* (lower row of pictures).

A

K14/K8/β-catenin/DAPI   K14/K8   β-catenin/DAPI   inset: β-catenin

K14-Cre
R26$^{EYFP/+}$

K14-Cre
β-catenin$^{f/+}$
Bmpr1a$^{f/f}$

50μm   10μm

B

day0   day4

EYFP   EYFP

K14-Cre
R26$^{EYFP/+}$

K14-Cre
β-catenin$^{f/+}$
Bmpr1a$^{f/f}$
R26$^{EYFP/+}$

K14-Cre
R26$^{EYFP/+}$ +MI-2   +MI-2

K14-Cre
β-catenin$^{f/+}$
Bmpr1a$^{f/f}$
R26$^{EYFP/+}$ +MI-2   +MI-2

100μm

C

K14-Cre
R26$^{EYFP/+}$

Viable organoids after 4 days, %

MI-2 - +

D

K14-Cre
β-catenin$^{f/+}$
Bmpr1a$^{f/f}$
R26$^{EYFP/+}$

Viable organoids after 4 days, %

MI-2 - +

E

H3K4me3/ DAPI   H3K4me3

K14-Cre
β-catenin$^{f/+}$
Bmpr1a$^{f/f}$

K14-Cre
β-catenin$^{f/+}$
Bmpr1a$^{f/f}$ + MI-2   + MI-2

20μm

F

H3K4me3

Fluorescence intensity

****

MI-2 - +

Figure 3. Mll1 Is Required for Tumor Maintenance in Mouse Salivary Gland Organoids: Pharmacological Interference

(A) After organoid formation, K14, K8, and β-catenin were stained by immunofluorescence: β-catenin was located at the membranes in controls (upper panel), while it was nuclear in organoids from double-mutant tumors.

(B) After their formation, control organoids and organoids from tumors were treated with the pharmacological inhibitor MI-2 at 2 μM, and the changes were monitored over time.

(C and D) Quantification of viable control (C) and tumor (D) organoids after 4 days of treatment. Error bars, mean ± SD. ***p < 0.001.

(E) Organoids from tumors were treated with MI-2 at 2 μM. H3K4me3 was stained by immunofluorescence.

(F) Quantification of viable fluorescence intensity of treated and untreated organoids. ****p < 0.0001. See also Figure S4.

gether, our genetic and pharmacological experiments showed that *Mll1* is essential for the initiation and maintenance of β-catenin^{GOF}; Bmpr1a^{LOF} salivary gland tumors and tumor-like organoids.

Conditional Mll1 Ablation Prevents Survival of Tumor-Propagating Cells in Salivary Gland Tumors

To assess mechanisms by which homozygous *Mll1* deletion prevents tumor formation in the salivary glands, we examined Wnt/β-catenin activity, cell differentiation, and apoptosis. In control salivary glands, β-catenin was located at the membranes in both K14- and K8-positive cells (Figure S4G, marked by white arrowheads). Triple-mutant salivary glands with heterozygous *Mll1* deletion on the tumor background exhibited nuclear β-catenin staining in many K14-positive tumor-propagating cells (Figures 4A, left column, marked by white arrowheads, and 4B, upper left two pictures). In contrast, none of the K14-positive cells in the epithelia of homozygous Mll1 triple-mutant glands showed nuclear staining of β-catenin (Figure 4A, right column, marked by cyan arrowheads). The differentiation marker K8 and β-catenin were located at the mem-
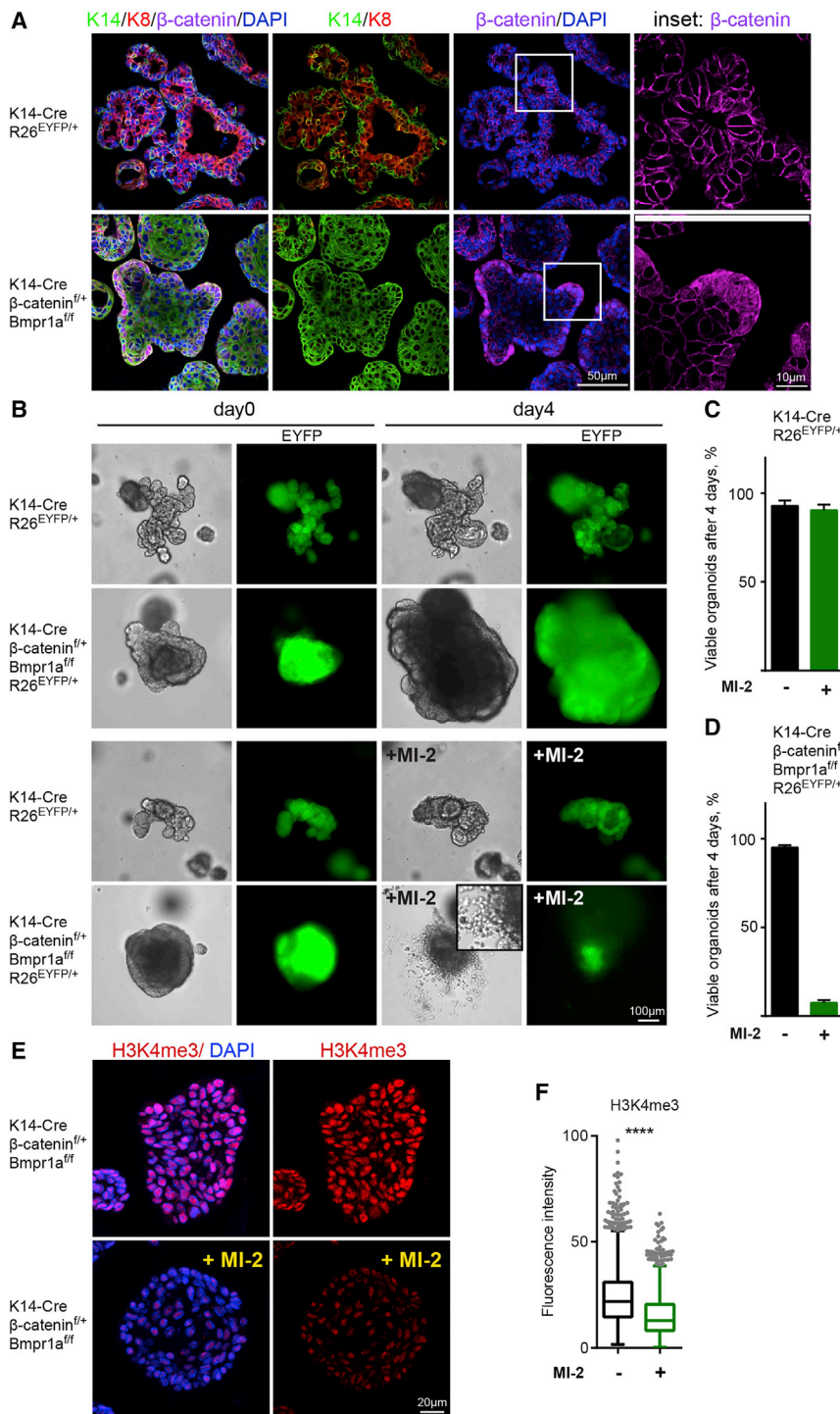
Figure 3C; Figure S4E, lower panel). In contrast, the growth of double-mutant organoids was strongly inhibited by MI-2 (Figure 3B, fourth panel, quantified in Figure 3D), and apoptosis was induced in the outer layer of the organoids (Figure S4F, lower panel). Inhibition of enzymatic activity of Mll1 with MI-2 reduced the level of H3K4me3 (Figures 3E and 3F). Alto-

branes (Figure 4B, upper two right pictures, marked by white arrowheads). Moreover, we observed increased apoptosis and reduced proliferation in the homozygous Mll1 triple-mutant glands, as shown by cleaved caspase-3 and Ki67 staining (Figure 4B, compare third and fourth right pictures with the left ones). These data show that Mll1 in the salivary gland tumors is required to
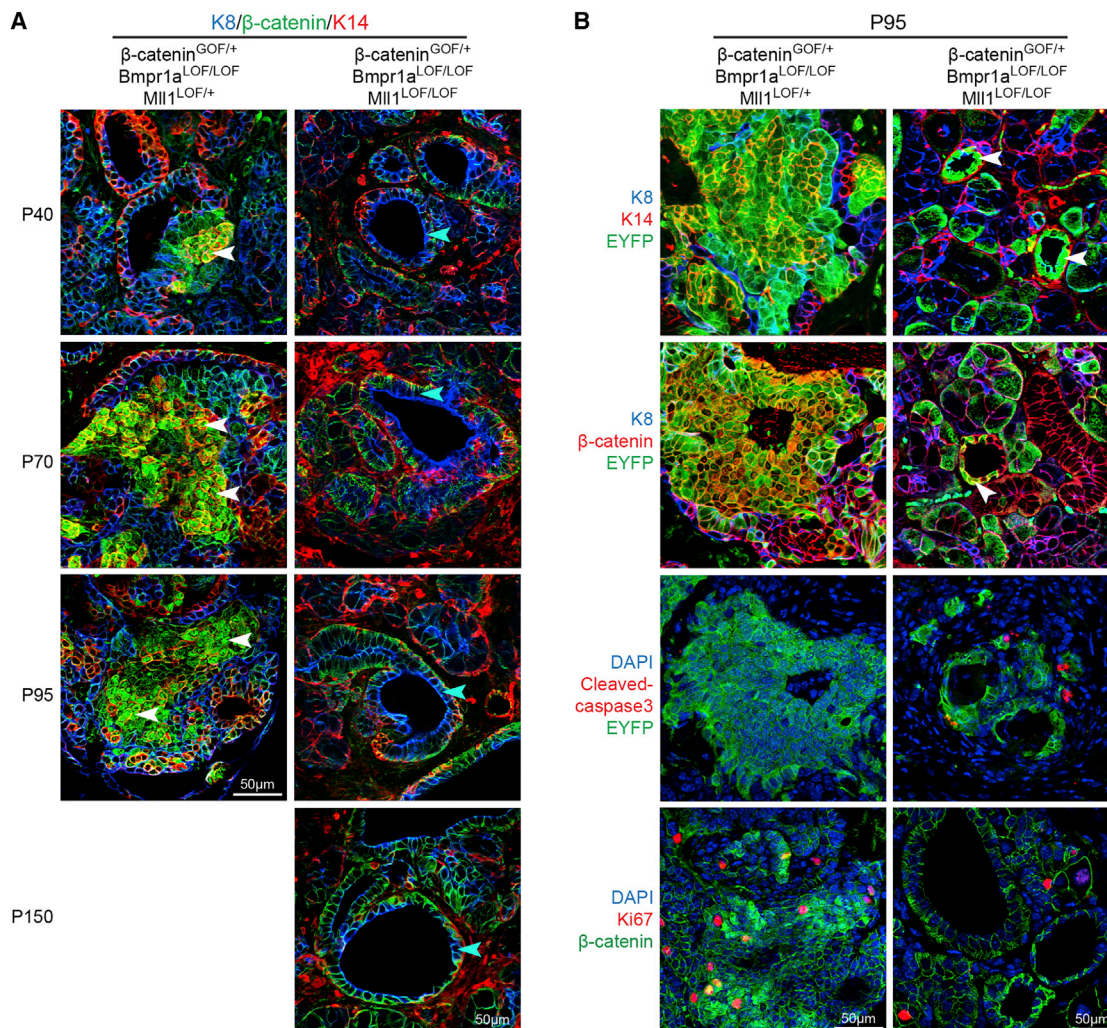
Figure 4. Mll1 Ablation in Salivary Gland Tumors Controls Differentiation and Apoptosis

(A) Immunofluorescence staining of K8, K14, and β-catenin in *Mll1*^f/+^ and *Mll1*^f/f^ salivary gland mutant mice on the tumor background at different stages.

(B) EYFP, cleaved caspase-3, and Ki67 staining of *Mll1*^f/+^ and *Mll1*^f/f^ mutant salivary glands on the tumor background.

sustain high Wnt activity and that *Mll1* ablation prevents the growth of poorly differentiated cells and impairs their survival.

Mll1 Deletion Inhibits Proliferation of Mouse and Human Head and Neck Cancer Cells

To further study the role of *Mll1* in head and neck cancer cells genetically, we carried out CRISPR/Cas9-based deletions in the primary mouse salivary gland SG257 cancer cells (Figure S1E) and in the human head and neck cancer cell line HNSCCUM-03T that exhibits high Wnt activity (Figure 6D) and elevated Mll1 activity and H3K4me3 modification in the sphere culture condition (Figures S6A and S6B) (Welkoborsky et al., 2003). Pairs of single-guide RNAs (sgRNAs) were designed to remove the essential exon 2 of mouse and human *Mll1* (Figures S5B and S5G). Over rounds of passaging, we observed the depletion of mouse and human cells that harbored *Mll1* mutant alleles, which were induced by the sgRNA pairs sgMll1-3/5 for mouse cells and sgMLL1-4/5 and sgMLL1-3/6 for human cells (Figures S5C,

S5H, and S5I) (see the percentages of stepwise reductions). Deletion of exon 2 of *Mll2* and *Mll3* by CRISPR/Cas9 had no significant influence on the growth of the mouse tumor cells (Figures S5J and S5K). To achieve a higher efficiency of deletion, we used mouse cell clone SG257 6, in which one *Mll1* allele had already been deleted (Figures S5D and S5F), to perform second-round deletions using the sgRNA pair sgMll1-4/6 (Figure S5B). During passaging, cells with homozygous deletion of *Mll1* were outcompeted: the percentage of *Mll1* mutant alleles fell from 94% to 50% (Figure S5E). Five days after transfection of salivary gland SG257 cell clone 6 with sgMll1-4/6, we observed cell-cycle arrest at the S phase (Figure S5L). These results indicate that *Mll1* is required for the growth of mouse and human tumor cells.

Mll1 Is Required for Tumor Initiation and Maintenance of Human Head and Neck Cancer Cells

To further investigate the importance of *Mll1* in human head and neck cancer cells and tumors, we generated heterozygous and
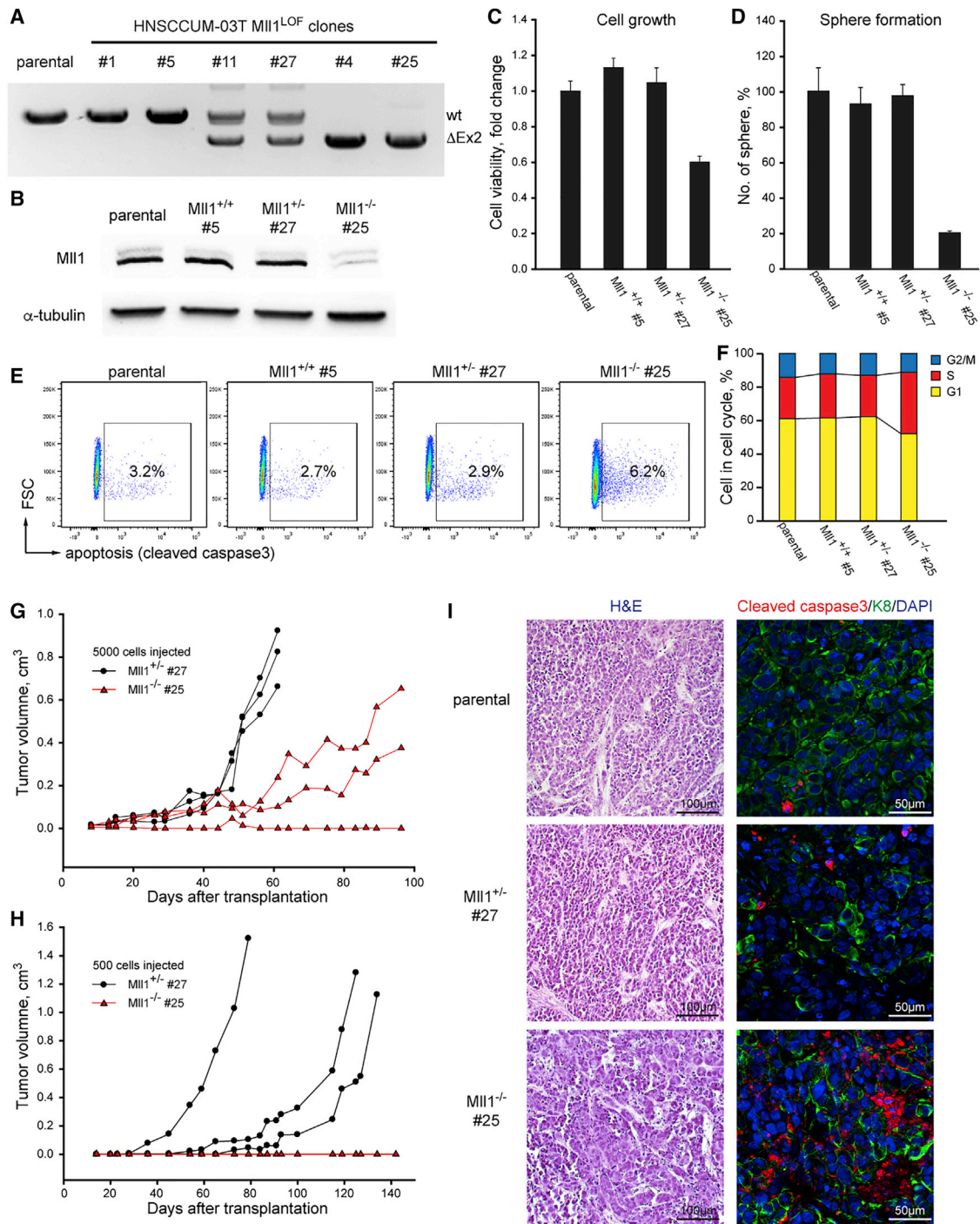
Figure 5. Deletion of Mll1 Reduces Tumorigenesis of Human Head and Neck Cancer Cells

(A and B) PCR (A) and western blotting (B) showed *Mll1* deletion in human HNSCCUM-03T cell clones 4 and 25.

(C and D) Influence of *Mll1* deletion on proliferation (C) and self-renewal (D) of HNSCCUM-03T cells measured using 3-(4,5-Dimethylthiazol-2-yl)-2,5-Diphenyltetrazolium Bromide (MTT) proliferation assays after 72 hr and sphere formation after 7 days. n = 3 independent experiments. Error bars, mean ± SD. ***p < 0.001 compared to parental cells.

(E and F) Apoptosis rate and cell-cycle distribution of *Mll1*$^{-/-}$ HNSCCUM-03T cells analyzed using cleaved caspase-3 (E) and propidium iodide (F) DNA staining.

(legend continued on next page)

homozygous *Mll1* knockout cell clones of HNSCCUM-03T cells by deleting the essential exon 2 (Figure S6C). *Mll1*$^{-/-}$ cell clones were viable and showed strongly reduced production of Mll1 protein (Figures 5A and 5B; Figure S5A). The cell growth of homozygous mutant cells was slightly impaired, while their sphere formation was strongly reduced (Figures 5C and 5D). *Mll1*$^{-/-}$ cells exhibited increased apoptosis and cell-cycle arrest at the S phase (Figures 5E and 5F). Gene expression profiling following *Mll1* ablation revealed silencing of *Mll1* target genes like *HOXA11*, *HOXA9*, and *HOXA10* (Figure S6D). In gene set enrichment analyses, *Mll1*$^{-/-}$ cells exhibited upregulated apoptosis and p53 signatures, along with downregulated cell-cycle genes and E2F targets (Figure S6E). To examine their tumor-propagating potential, *Mll1*$^{+/-}$ and *Mll1*$^{-/-}$ cells were injected into the back skin of NOD-SCID mice: *Mll1*$^{+/-}$ cells produced fast-growing tumors upon injection of 500 or 5,000 cells, while *Mll1*$^{-/-}$ cells required higher numbers of cells to initiate tumorigenesis, and these tumors grew more slowly (Figures 5G and 5H). In tumors formed by *Mll1*$^{-/-}$ cells, we observed increased apoptosis and reduced proliferation (Figure 5I; Figure S6F). Overall, our data show that the deletion of *Mll1* reduces proliferation and increases apoptosis of mouse salivary gland and human head and neck cancer cells and thus reduces tumorigenesis.

Pharmacological Interference with the β-Catenin-Mll1 Complex Affects Tumor-Propagating Cells' Self-Renewal

To exert their functions as modulators of gene expression, both Mll1 and β-catenin form multi-protein complexes (scheme in Figure 6A). Menin is a direct N-terminal binding partner of Mll1 and its fusion proteins and is required for the regulation of target genes and leukemogenesis (Yokoyama et al., 2005). BRD4 is an epigenetic reader of lysine acetylation that synergizes with Mll1 fusion proteins at HOX loci to promote leukemogenesis (Dawson et al., 2011; Muntean et al., 2010). Mll1 interacts indirectly with β-catenin via CBP (Arai et al., 2010), and β-catenin binds to DNA through TCF-LEF factors (Behrens et al., 1996; Fasolini et al., 2003). To assess the importance of these protein partners on Mll1 function, we examined sphere formation in the salivary gland SG257 cells (Figure S1E) in the presence of the Mll1/Menin interaction inhibitor MI-2 (Grembecka et al., 2012), the BRD4 inhibitor JQ1 (Grembecka et al., 2012), the β-catenin/CBP interaction inhibitor ICG-001 (Emami et al., 2004), the β-catenin/TCF4 interaction inhibitor LF3 (Fang et al., 2016), and the CBP histone acetyltransferase enzyme activity inhibitor C646 and bromodomain inhibitor I-CBP112 (Bowers et al., 2010; Picaud et al., 2015). In all cases except C646 and I-CBP112, the inhibitors blocked the formation of spheres of mouse salivary gland tumor cells in concentration-dependent manners (Figure 6B). This shows that protein-protein interactions of Mll1 to the partner molecules are crucial for the Mll1

function but that the CBP enzyme activity is not crucial: CBP seems to mediate the link between β-catenin and Mll1.

To test whether this holds true in human HNSCCs, we included further human HNSCC cell lines. The expression of *AXIN2* and *HOXA9* was measured to indicate Wnt and Mll1 activity, respectively. Among 9 cell lines, 4 of them have relatively high Wnt activity and 3 of them have high *HOXA9* expression (Figures S7A and S7B), suggesting the Wnt and Mll1 activation is common among human HNSCCs. Immunoprecipitation confirmed that Mll1 and the β-catenin transcription factor complex interact in HNSCCUM-03T sphere cells and that ICG-001 and LF3 interfered in the expected manner (Figures S7C and S7D; compare with mouse cells in Figures S3C and S3D). We tested the therapeutic potential of the inhibitors on HNSCCUM-03T high Wnt cells, which possess a higher sphere-forming ability but have a proliferating rate similar to that of HNSCCUM-02T cells that show low Wnt activity (Figure 6C; Figure S7E) (Welkoborsky et al., 2003). Sphere formation of HNSCCUM-03T cells was strongly inhibited when treated with the interfering compounds MI-2, JQ1, ICG-001, and LF3 (Figure 6C). Secondary sphere-formation assays were performed to confirm the loss-of-self-renewal phenotype (Figure S7F). In contrast, HNSCCUM-02T and SCC4 cells, which exhibit low Wnt activity, were less sensitive to the interfering compounds (Figures 6D and 6E). These results show that physical interactions between Mll1 and various partners, including β-catenin, are critical to the support the self-renewal capacity of Wnt-dependent human tumor-propagating cells.

Protein-Protein Interaction Domains and the SET Enzyme Activity of Mll1 Play Crucial Roles

Mll1 requires specific interactions with partner molecules and the histone methyltransferase activity for H3K4 of the su(var)3-9, enhancer-of-zeste and trithorax (SET) domain (Figure 6A). In particular, high SET activity requires the multiple protein partners of Mll1; of these, WDR5 is required specifically by Mll1 (Li et al., 2016; Southall et al., 2009). To examine whether these partner proteins and the methyltransferase activity of the SET domain are required for maintaining tumor-propagating cells, we used a modified procedure developed by Shi and collaborators (Shi et al., 2015) (Figure 7A). This involved first introducing a Cas9-mCherry expression cassette into the mouse SG257 and human HNSCCUM-03T cells by a transposon system. Then mCherry$^+$ cells were enriched by FACS and mixed with non-colored parental cells. Next, a lentiviral-based construct was used to express different sgRNAs and a Puromycin-resistance gene (Figure 7A). Specific sgRNAs targeted the essential amino acids of Mll1: F9; L2838/I2842 in mouse and L2848/I2852 in human cells; R3759 in mouse and R3768 in human cells, which conduct Mll1/Menin, Mll1/CBP, and Mll1/WDR5 interactions; and the essential SET active site amino acids Y3852/Y3936 in mouse and Y3861/Y3945 in human cells, along

---

(G and H) *Mll1*$^{+/-}$ and *Mll1*$^{-/-}$ HNSCCUM-03T cells (5,000, G, or 500, H) were transplanted into the back skin of NOD-SCID mice to examine the effect of *Mll1* deletion on tumor initiation ability.

(I) (Left) Histological comparison between tumor xenografts initiated by parental, *Mll1*$^{+/-}$, and *Mll1*$^{-/-}$ HNSCCUM-03T cells. (Right) Cleaved caspase-3 staining shows the apoptosis rate of the different cells.

See also Figures S5 and S6.
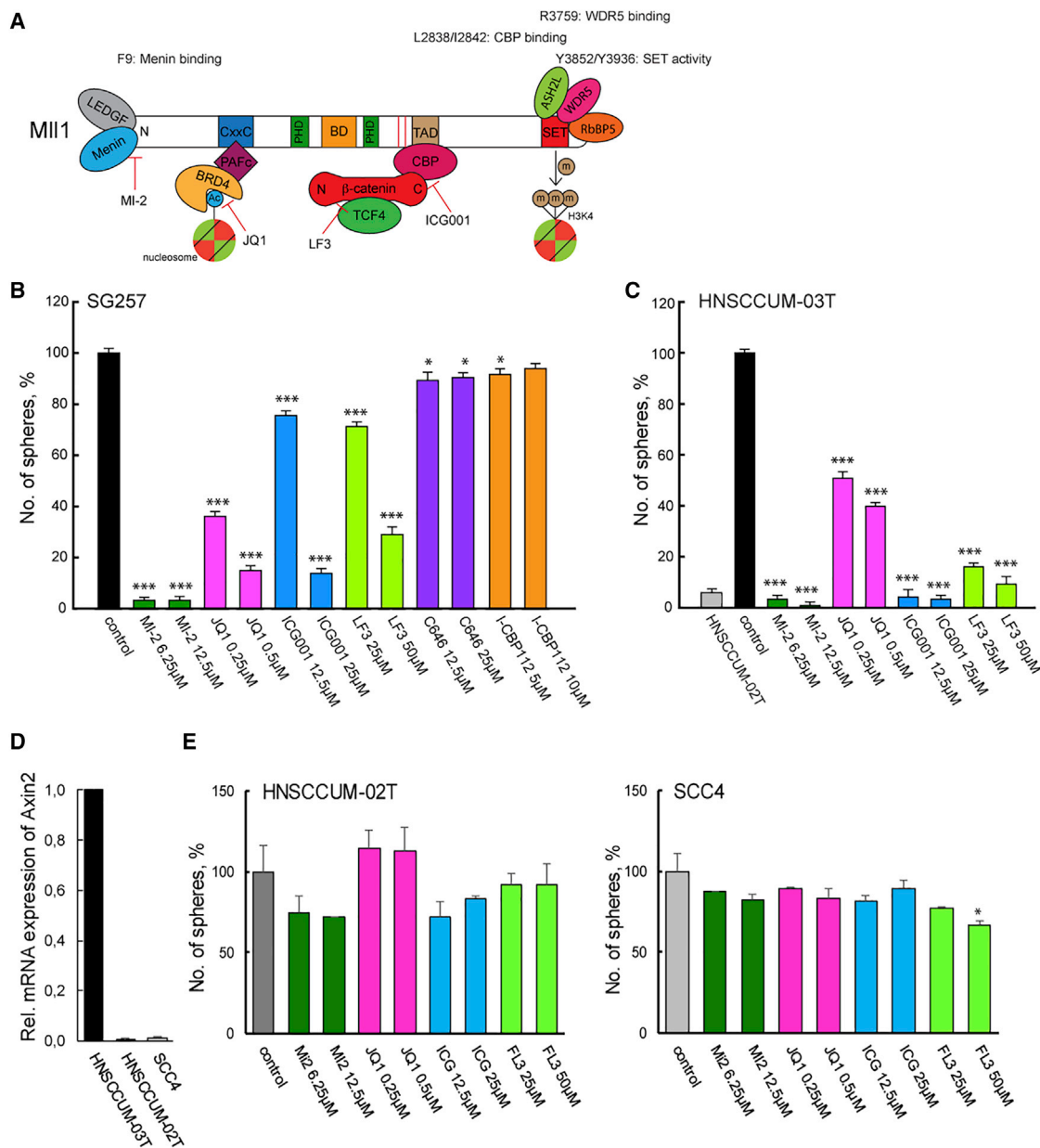
Figure 6. Targeting the β-Catenin/CBP/Mll1 Complex in Tumor-Propagating Cells by Small Molecule Inhibitors

(A) Scheme of the action of small molecule inhibitors targeting the β-catenin/CBP/Mll1 complex.

(B and C) Sphere-formation assays used to determine the influence of individual inhibitors on the self-renewal of mouse salivary gland SG257 cancer cells (B) and human HNSCCUM-03T high Wnt head and cancer cells (C).

(D and E) Human HNSCCUM-02T and SCC4 low Wnt head and neck cancer cells with low self-renewal ability (D) and with no or less sensitivity to inhibitors (E).

n = 3 independent experiments. Error bars, mean ± SD. ***p < 0.001, *p < 0.05 compared to control.

See also Figure S7.

with several neighboring non-essential sites (De Guzman et al., 2006; Huang et al., 2012; Song and Kingston, 2008; Southall et al., 2009). After Puromycin selection, mutant cells were subjected to sphere culture for 10 days, and FACS was used to analyze the ratios of mCherry+ cells.

We found that sgRNAs targeting regions of essential amino acids of Mll1 effectively depleted mouse and human tumor-

propagating cells in sphere culture (Figures 7B and 7C, red bars). In contrast, sgRNAs targeting regions neighboring these essential sites caused only minimal negative-selection phenotypes (black bars). Next-generation sequencing was used to measure the abundance of the mutations after CRISPR/Cas9 editing: in-frame deletion mutations outcompeted frameshift mutations when generated adjacent to the non-essential amino

A

Transposon insertion + FACS

Lentiviral induction + selection
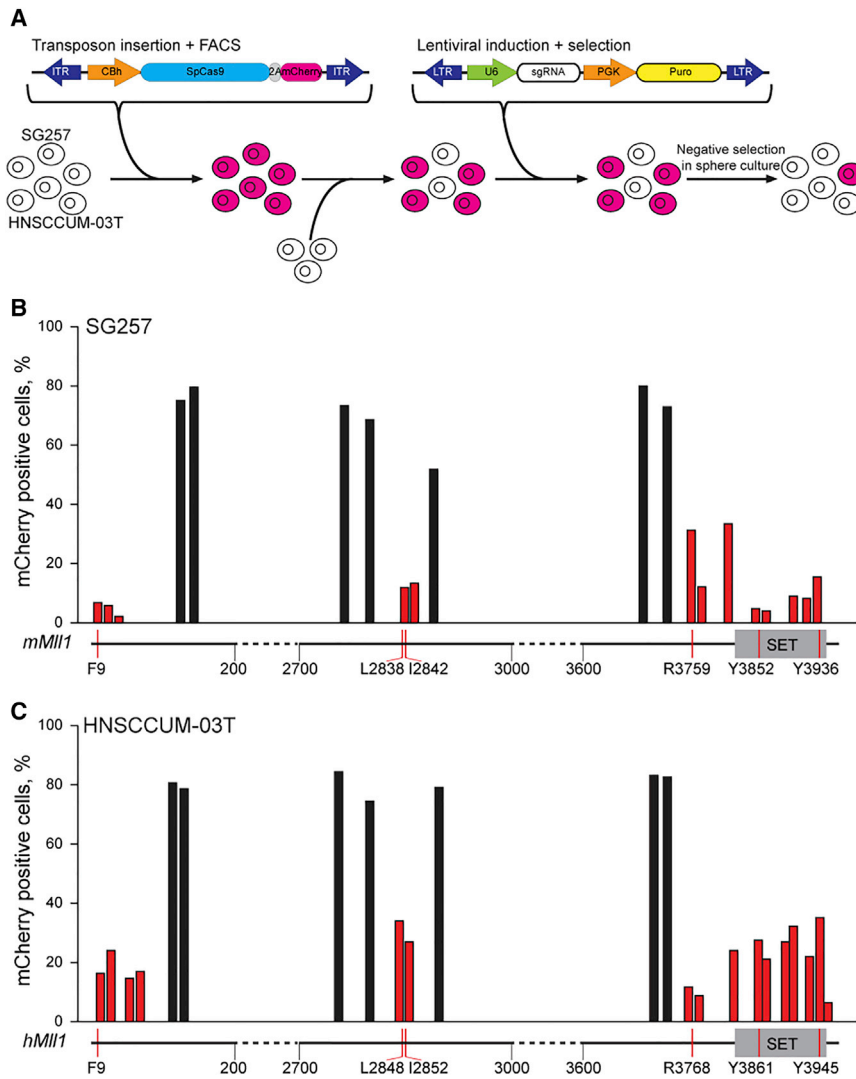
Figure 7. CRISPR/Cas-Based Domain Mutagenesis of Mll1

(A) Procedure of CRISPR/Cas-based domain mutagenesis, sphere culture, and mCherry analyses.

(B and C) Cas9-mCherry+ cells in mouse SG257 cells (B) and human HNSCCUM-03T cells (C) after introduction of essential Mll1 mutations (orange bars) and neighboring non-essential ones (black bars) using various sgRNAs.

See also Figure S7.

B SG257

C HNSCCUM-03T

with transcriptional activation. These results suggest that highly activated Wnt/β-catenin signaling is linked to global chromatin opening through H3K4 tri-methylation in salivary gland and head and neck cancers. Moreover, genes involved in cytokine production pathways showed elevated levels of H3K4me2 and H3K4me3 modification, including *Il1a*, *Il23a*, and *Cxcr2*, which, along with their family members, are well-known cytokines that participate in the remodeling of the tumor microenvironment critical for tumor initiation and progression (Holland et al., 2013; Katoh et al., 2013; Langowski et al., 2006; Wolf et al., 2001). This indicates that in tumor-propagating cells, Mll1 may have specific roles in the regulation of the tumor microenvironment by changing the cytokine production.

Mll1 mutations are reported in more than 70% of acute leukemia in infants and in 5%–10% of acute lymphoblastic leukemia in adults (Winters and Bernt, 2017), indicating its essential roles in hematopoietic tumors. *Mll1* is mutated in

acids (Figure S7C, left). When generated adjacent to essential amino acids, the ratio between the two mutation forms remained the same (Figure S7C, right). Collectively, these findings show that the SET enzyme activity and the Mll1/Menin, Mll1/CBP/β-catenin and Mll1/WDR5 interactions are essential for the functions of Mll1 in promoting the growth and survival of tumor-propagating cells of the mouse salivary gland and human head and neck tumor cells.

DISCUSSION

Global opening in the chromatin landscape has been shown in embryonic and leukemia stem cells (Wong et al., 2015; Zoncu et al., 2011). Relaxed chromatin structure, which is often associated with transcriptional activation, is characterized by enrichment of specific histone modifications such as H3K4 tri-methylation. Our ChIP-seq and mRNA-seq data showed that salivary gland tumor-propagating cells possess a globally elevated level of H3K4me3 that is enriched at promoters and is associated

5.7% of human head and neck cancers (Cancer Genome Atlas Network, 2015). Our data show that Mll1 is upregulated in tumor-propagating cells of salivary gland and head and neck cancers, and this is supported by high Wnt activity. Deletion of Mll1 impairs the tumorigenesis significantly. This demonstrates that Mll1 is also involved in the biology of solid tumors and mainly regulated through transcriptional activation, which is supported by other studies performed with cell cultures and xenografted tumor cells (Ansari et al., 2013; Gallo et al., 2013; Heddleston et al., 2012; Malik et al., 2015; Tamura et al., 2014; Zhu et al., 2015). Here we provide genetic evidence that ablation of Mll1 blocks Wnt/β-catenin-driven tumorigenesis and show that Mll1 acts downstream of Wnt/β-catenin to control self-renewal, proliferation, and apoptosis of salivary gland and head and neck cancer. Moreover, we developed a unique organoid model system to confirm Mll1 as a critical regulator for both initiation and maintenance of salivary gland tumors.

In hematopoietic cancers, the N-terminal part of *Mll1* undergoes translocations to many partner molecules, suggesting

that this region has crucial functions (Ayton and Cleary, 2001; Dou and Hess, 2008; Meyer et al., 2013). Studies revealed that leukemogenesis also requires the wild-type *Mll1* allele, indicating that the C-terminal domain is essential in leukemia (Thiel et al., 2010). Our data obtained using CRISPR/Cas9-mediated mutagenesis of both the essential interaction sites of Mll1 and the SET enzyme active site strongly reduced self-renewal of human and mouse tumor-propagating cells. These results demonstrate that both N- and C-terminal regions of Mll1 are functionally important in these solid cancers.

Given that small molecule inhibitors targeting Mll1 have been pursued in the potential therapy for MLL-associated leukemia (Cao et al., 2014), we envision that a similar strategy might cause tumor impairment of human salivary gland and head and neck cancer. Moreover, our data from menin inhibitor-2 (MI-2)-treated control and tumor organoids demonstrated that malignant cells were more sensitive than non-malignant cells to Mll1 inhibition, indicating that targeting Mll1 might be a promising strategy to inhibit these tumor cells. Whether combinations of Wnt and Mll1 inhibitors synergize in solid cancers is a question for subsequent studies. Our salivary gland tumor organoids could also facilitate the identification of further reagents with therapeutic potential.

Altogether, our study demonstrates that a further layer of regulation acts downstream of Wnt/β-catenin in salivary gland and head and neck cancer. This involves Mll1 action and H3K4me3, which appear to trigger the opening of chromatin that is required for promoting stem cell programs. In the future, small molecule inhibitors that are able to target specific Mll1 functions could offer a promising direction for the development of therapies to treat this important class of aggressive human diseases.

STAR★METHODS

Detailed methods are provided in the online version of this paper and include the following:

- KEY RESOURCES TABLE
- CONTACT FOR REAGENT AND RESOURCE SHARING
- EXPERIMENTAL MODEL AND SUBJECT DETAILS
  - Cell culture
  - Mice
- METHOD DETAILS
  - ChIP-Seq and mRNA-seq
  - Compounds
  - CRISPR/Cas-based Gene Deletion and Domain Mutagenesis
  - Immunofluorescence and other Stainings
  - Quantitative Real-Time PCR
  - Immunoprecipitation and Western Blotting
  - Organoid Culture
  - Cell Cycle and Apoptosis Analyses
  - Xenotransplantation Studies
  - Gene Expression Profiling by Microarray
  - ChIP-seq and mRNA-seq Data Analysis
  - Mutation Abundance Measurement by NGS
- QUANTIFICATION AND STATISTICAL ANALYSIS
- DATA AND SOFTWARE AVAILABILITY

REFERENCES

Alioto, T.S., Buchhalter, I., Derdak, S., Hutter, B., Eldridge, M.D., Hovig, E., Heisler, L.E., Beck, T.A., Simpson, J.T., Tonon, L., et al. (2015). A comprehensive assessment of somatic mutation detection in cancer using whole-genome sequencing. Nat. Commun. *6*, 10001.

Ansari, K.I., Kasiri, S., and Mandal, S.S. (2013). Histone methylase MLL1 has critical roles in tumor growth and angiogenesis and its knockdown suppresses tumor growth *in vivo*. Oncogene *32*, 3359–3370.

Arai, M., Dyson, H.J., and Wright, P.E. (2010). Leu628 of the KIX domain of CBP is a key residue for the interaction with the MLL transactivation domain. FEBS Lett. *584*, 4500–4504.

Ayton, P.M., and Cleary, M.L. (2001). Molecular mechanisms of leukemogenesis mediated by MLL fusion proteins. Oncogene *20*, 5695–5707.

Bauml, J.M., Cohen, R.B., and Aggarwal, C. (2016). Immunotherapy for head and neck cancer: latest developments and clinical potential. Ther. Adv. Med. Oncol. *8*, 168–175.

Behrens, J., von Kries, J.P., Kühl, M., Bruhn, L., Wedlich, D., Grosschedl, R., and Birchmeier, W. (1996). Functional interaction of beta-catenin with the transcription factor LEF-1. Nature *382*, 638–642.

Bowers, E.M., Yan, G., Mukherjee, C., Orry, A., Wang, L., Holbert, M.A., Crump, N.T., Hazzalin, C.A., Liszczak, G., Yuan, H., et al. (2010). Virtual ligand screening of the p300/CBP histone acetyltransferase: identification of a selective small molecule inhibitor. Chem. Biol. *17*, 471–482.

Campbell, J.D., Yau, C., Bowlby, R., Liu, Y., Brennan, K., Fan, H., Taylor, A.M., Wang, C., Walter, V., Akbani, R., et al. (2018). Genomic, pathway network, and immunologic features distinguishing squamous carcinomas. Cell Rep. *23*, 194–212.

Cancer Genome Atlas Network (2015). Comprehensive genomic characterization of head and neck squamous cell carcinomas. Nature *517*, 576–582.

Cao, F., Townsend, E.C., Karatas, H., Xu, J., Li, L., Lee, S., Liu, L., Chen, Y., Ouillette, P., Zhu, J., et al. (2014). Targeting MLL1 H3K4 methyltransferase activity in mixed-lineage leukemia. Mol. Cell *53*, 247–261.

Chen, Y., Anastassiadis, K., Kranz, A., Stewart, A.F., Arndt, K., Waskow, C., Yokoyama, A., Jones, K., Neff, T., Lee, Y., and Ernst, P. (2017). MLL2, Not MLL1, Plays a Major Role in Sustaining MLL-Rearranged Acute Myeloid Leukemia. Cancer Cell 31, 755–770.

Chu, P.G., and Weiss, L.M. (2002). Keratin expression in human tissues and neoplasms. Histopathology 40, 403–439.

Clevers, H. (2016). Modeling development and disease with organoids. Cell 165, 1586–1597.

Dawson, M.A., Prinjha, R.K., Dittmann, A., Giotopoulos, G., Bantscheff, M., Chan, W.I., Robson, S.C., Chung, C.W., Hopf, C., Savitski, M.M., et al. (2011). Inhibition of BET recruitment to chromatin as an effective treatment for MLL-fusion leukaemia. Nature 478, 529–533.

De Guzman, R.N., Goto, N.K., Dyson, H.J., and Wright, P.E. (2006). Structural basis for cooperative transcription factor binding to the CBP coactivator. J. Mol. Biol. 355, 1005–1013.

Díaz Prado, S.M., Medina Villaamil, V., Aparicio Gallego, G., Blanco Calvo, M., López Cedrún, J.L., Sironvalle Soliva, S., Valladares Ayerbes, M., García Campelo, R., and Antón Aparicio, L.M. (2009). Expression of Wnt gene family and frizzled receptors in head and neck squamous cell carcinomas. Virchows Arch. 455, 67–75.

Dobin, A., Davis, C.A., Schlesinger, F., Drenkow, J., Zaleski, C., Jha, S., Batut, P., Chaisson, M., and Gingeras, T.R. (2013). STAR: ultrafast universal RNA-seq aligner. Bioinformatics 29, 15–21.

Dou, Y., and Hess, J.L. (2008). Mechanisms of transcriptional regulation by MLL and its disruption in acute leukemia. Int. J. Hematol. 87, 10–18.

Emami, K.H., Nguyen, C., Ma, H., Kim, D.H., Jeong, K.W., Eguchi, M., Moon, R.T., Teo, J.L., Kim, H.Y., Moon, S.H., et al. (2004). A small molecule inhibitor of beta-catenin/CREB-binding protein transcription [corrected]. Proc. Natl. Acad. Sci. USA 101, 12682–12687.

Ernst, P., Wang, J., Huang, M., Goodman, R.H., and Korsmeyer, S.J. (2001). MLL and CREB bind cooperatively to the nuclear coactivator CREB-binding protein. Mol. Cell. Biol. 21, 2249–2258.

Fang, L., Zhu, Q., Neuenschwander, M., Specker, E., Wulf-Goldenberg, A., Weis, W.I., von Kries, J.P., and Birchmeier, W. (2016). A small-molecule antagonist of the β-catenin/TCF4 interaction blocks the self-renewal of cancer stem cells and suppresses tumorigenesis. Cancer Res. 76, 891–901.

Fasolini, M., Wu, X., Flocco, M., Trosset, J.Y., Oppermann, U., and Knapp, S. (2003). Hot spots in Tcf4 for the interaction with beta-catenin. J. Biol. Chem. 278, 21092–21098.

Gallo, M., Ho, J., Coutinho, F.J., Vanner, R., Lee, L., Head, R., Ling, E.K., Clarke, I.D., and Dirks, P.B. (2013). A tumorigenic MLL-homeobox network in human glioblastoma stem cells. Cancer Res. 73, 417–427.

Grembecka, J., He, S., Shi, A., Purohit, T., Muntean, A.G., Sorenson, R.J., Showalter, H.D., Murai, M.J., Belcher, A.M., Hartley, T., et al. (2012). Menin-MLL inhibitors reverse oncogenic activity of MLL fusion proteins in leukemia. Nat. Chem. Biol. 8, 277–284.

Harada, N., Tamai, Y., Ishikawa, T., Sauer, B., Takaku, K., Oshima, M., and Taketo, M.M. (1999). Intestinal polyposis in mice with a dominant stable mutation of the beta-catenin gene. EMBO J. 18, 5931–5942.

Haraguchi, K., Ohsugi, M., Abe, Y., Semba, K., Akiyama, T., and Yamamoto, T. (2008). Ajuba negatively regulates the Wnt signaling pathway by promoting GSK-3beta-mediated phosphorylation of beta-catenin. Oncogene 27, 274–284.

Hashimshony, T., Senderovich, N., Avital, G., Klochendler, A., de Leeuw, Y., Anavy, L., Gennert, D., Li, S., Livak, K.J., Rozenblatt-Rosen, O., et al. (2016). CEL-Seq2: sensitive highly-multiplexed single-cell RNA-seq. Genome Biol. 17, 77.

Heddleston, J.M., Wu, Q., Rivera, M., Minhas, S., Lathia, J.D., Sloan, A.E., Iliopoulos, O., Hjelmeland, A.B., and Rich, J.N. (2012). Hypoxia-induced mixed-lineage leukemia 1 regulates glioma stem cell tumorigenic potential. Cell Death Differ. 19, 428–439.

Hoesli, R.C., Ludwig, M.L., Michmerhuizen, N.L., Rosko, A.J., Spector, M.E., Brenner, J.C., and Birkeland, A.C. (2017). Genomic sequencing and precision medicine in head and neck cancers. Eur. J. Surg. Oncol. 43, 884–892.

Holland, J.D., Gyorffy, B., Vogel, R., Eckert, K., Valenti, G., Fang, L., Lohneis, P., Elezkurtaj, S., Ziebold, U., and Birchmeier, W. (2013). Combined Wnt/beta-catenin, Met, and CXCL12/CXCR4 signals characterize basal breast cancer and predict disease outcome. Cell Rep 5, 1214–1227.

Huang, J., Gurung, B., Wan, B., Matkar, S., Veniaminova, N.A., Wan, K., Merchant, J.L., Hua, X., and Lei, M. (2012). The same pocket in menin binds both MLL and JUND but has opposite effects on transcription. Nature 482, 542–546.

Huelsken, J., Vogel, R., Erdmann, B., Cotsarelis, G., and Birchmeier, W. (2001). Beta-catenin controls hair follicle morphogenesis and stem cell differentiation in the skin. Cell 105, 533–545.

Jäckel, M.C., and Scheckenbach, K. (2014). [Good local control by supracricoid partial laryngectomy (SCPL)]. Laryngorhinootologie 93, 504–505.

Katase, N., Lefeuvre, M., Gunduz, M., Gunduz, E., Beder, L.B., Grenman, R., Fujii, M., Tamamura, R., Tsujigiwa, H., and Nagatsuka, H. (2012). Absence of Dickkopf (Dkk)-3 protein expression is correlated with longer disease-free survival and lower incidence of metastasis in head and neck squamous cell carcinoma. Oncol. Lett. 3, 273–280.

Katoh, H., Wang, D., Daikoku, T., Sun, H., Dey, S.K., and Dubois, R.N. (2013). CXCR2-expressing myeloid-derived suppressor cells are essential to promote colitis-associated tumorigenesis. Cancer Cell 24, 631–644.

Konings, A.W., Faber, H., Cotteleer, F., Vissink, A., and Coppes, R.P. (2006). Secondary radiation damage as the main cause for unexpected volume effects: a histopathologic study of the parotid gland. Int. J. Radiat. Oncol. Biol. Phys. 64, 98–105.

Kranz, A., Fu, J., Duerschke, K., Weidlich, S., Naumann, R., Stewart, A.F., and Anastassiadis, K. (2010). An improved Flp deleter mouse in C57Bl/6 based on Flpo recombinase. Genesis 48, 512–520.

Kwon, C., Cheng, P., King, I.N., Andersen, P., Shenje, L., Nigam, V., and Srivastava, D. (2011). Notch post-translationally regulates β-catenin protein in stem and progenitor cells. Nat. Cell Biol. 13, 1244–1251.

Langowski, J.L., Zhang, X., Wu, L., Mattson, J.D., Chen, T., Smith, K., Basham, B., McClanahan, T., Kastelein, R.A., and Oft, M. (2006). IL-23 promotes tumour incidence and growth. Nature 442, 461–465.

Leemans, C.R., Braakhuis, B.J., and Brakenhoff, R.H. (2011). The molecular biology of head and neck cancer. Nat. Rev. Cancer 11, 9–22.

Li, Y., Han, J., Zhang, Y., Cao, F., Liu, Z., Li, S., Wu, J., Hu, C., Wang, Y., Shuai, J., et al. (2016). Structural basis for activity regulation of MLL family methyltransferases. Nature 530, 447–452.

Lustig, B., Jerchow, B., Sachs, M., Weiler, S., Pietsch, T., Karsten, U., van de Wetering, M., Clevers, H., Schlag, P.M., Birchmeier, W., and Behrens, J. (2002). Negative feedback loop of Wnt signaling through upregulation of conductin/axin2 in colorectal and liver tumors. Mol. Cell. Biol. 22, 1184–1193.

Maimets, M., Rocchi, C., Bron, R., Pringle, S., Kuipers, J., Giepmans, B.N., Vries, R.G., Clevers, H., de Haan, G., van Os, R., and Coppes, R.P. (2016). Long-term in vitro expansion of salivary gland stem cells driven by Wnt signals. Stem Cell Reports 6, 150–162.

Malik, R., Khan, A.P., Asangani, I.A., Cieślik, M., Prensner, J.R., Wang, X., Iyer, M.K., Jiang, X., Borkin, D., Escara-Wilke, J., et al. (2015). Targeting the MLL complex in castration-resistant prostate cancer. Nat. Med. 21, 344–352.

Matuschek, C., Bölke, E., Geigis, C., Kammers, K., Ganswindt, U., Scheckenbach, K., Gripp, S., Simiantonakis, J., Hoffmann, T.K., Greve, J., et al. (2016). Influence of dosimetric and clinical criteria on the requirement of artificial nutrition during radiotherapy of head and neck cancer patients. Radiother. Oncol. 120, 28–35.

Meyer, C., Hofmann, J., Burmeister, T., Gröger, D., Park, T.S., Emerenciano, M., Pombo de Oliveira, M., Renneville, A., Villarese, P., Macintyre, E., et al. (2013). The MLL recombinome of acute leukemias in 2013. Leukemia 27, 2165–2176.

Mishina, Y., Hanks, M.C., Miura, S., Tallquist, M.D., and Behringer, R.R. (2002). Generation of Bmpr/Alk3 conditional knockout mice. Genesis *32*, 69–72.

Morris, L.G., Kaufman, A.M., Gong, Y., Ramaswami, D., Walsh, L.A., Turcan, Ş., Eng, S., Kannan, K., Zou, Y., Peng, L., et al. (2013). Recurrent somatic mutation of FAT1 in multiple human cancers leads to aberrant Wnt activation. Nat. Genet. *45*, 253–261.

Morris, L.G.T., Chandramohan, R., West, L., Zehir, A., Chakravarty, D., Pfister, D.G., Wong, R.J., Lee, N.Y., Sherman, E.J., Baxi, S.S., et al. (2017). The molecular landscape of recurrent and metastatic head and neck cancers: insights from a precision oncology sequencing platform. JAMA Oncol. *3*, 244–255.

Mountzios, G., Rampias, T., and Psyrri, A. (2014). The mutational spectrum of squamous-cell carcinoma of the head and neck: targetable genetic events and clinical impact. Ann. Oncol. *25*, 1889–1900.

Muntean, A.G., Tan, J., Sitwala, K., Huang, Y., Bronstein, J., Connelly, J.A., Basrur, V., Elenitoba-Johnson, K.S., and Hess, J.L. (2010). The PAF complex synergizes with MLL fusion proteins at HOX loci to promote leukemogenesis. Cancer Cell *17*, 609–621.

Picaud, S., Fedorov, O., Thanasopoulou, A., Leonards, K., Jones, K., Meier, J., Olzscha, H., Monteiro, O., Martin, S., Philpott, M., et al. (2015). Generation of a selective small molecule inhibitor of the CBP/p300 bromodomain for leukemia therapy. Cancer Res. *75*, 5106–5119.

Pinello, L., Canver, M.C., Hoban, M.D., Orkin, S.H., Kohn, D.B., Bauer, D.E., and Yuan, G.C. (2016). Analyzing CRISPR genome-editing experiments with CRISPResso. Nat. Biotechnol *24*, 695–697.

Prince, M.E., Sivanandan, R., Kaczorowski, A., Wolf, G.T., Kaplan, M.J., Dalerba, P., Weissman, I.L., Clarke, M.F., and Ailles, L.E. (2007). Identification of a subpopulation of cells with cancer stem cell properties in head and neck squamous cell carcinoma. Proc. Natl. Acad. Sci. USA *104*, 973–978.

Ran, F.A., Hsu, P.D., Wright, J., Agarwala, V., Scott, D.A., and Zhang, F. (2013). Genome engineering using the CRISPR-Cas9 system. Nat. Protoc. *8*, 2281–2308.

Salz, T., Li, G., Kaye, F., Zhou, L., Qiu, Y., and Huang, S. (2014). hSETD1A regulates Wnt target genes and controls tumor growth of colorectal cancer cells. Cancer Res. *74*, 775–786.

Sanjana, N.E., Shalem, O., and Zhang, F. (2014). Improved vectors and genome-wide libraries for CRISPR screening. Nat. Methods *11*, 783–784.

Shi, J., Wang, E., Milazzo, J.P., Wang, Z., Kinney, J.B., and Vakoc, C.R. (2015). Discovery of cancer drug targets by CRISPR-Cas9 screening of protein domains. Nat. Biotechnol. *33*, 661–667.

Sierra, J., Yoshida, T., Joazeiro, C.A., and Jones, K.A. (2006). The APC tumor suppressor counteracts beta-catenin activation and H3K4 methylation at Wnt target genes. Genes Dev. *20*, 586–600.

Song, J.J., and Kingston, R.E. (2008). WDR5 interacts with mixed lineage leukemia (MLL) protein via the histone H3-binding pocket. J. Biol. Chem. *283*, 35258–35264.

Southall, S.M., Wong, P.S., Odho, Z., Roe, S.M., and Wilson, J.R. (2009). Structural basis for the requirement of additional factors for MLL1 SET domain activity and recognition of epigenetic marks. Mol. Cell *33*, 181–191.

Srinivas, S., Watanabe, T., Lin, C.S., William, C.M., Tanabe, Y., Jessell, T.M., and Costantini, F. (2001). Cre reporter strains produced by targeted insertion of EYFP and ECFP into the ROSA26 locus. BMC Dev. Biol. *1*, 4.

Takemaru, K.I., and Moon, R.T. (2000). The transcriptional coactivator CBP interacts with beta-catenin to activate gene expression. J. Cell Biol. *149*, 249–254.

Tamura, M., Sasaki, Y., Koyama, R., Takeda, K., Idogawa, M., and Tokino, T. (2014). Forkhead transcription factor FOXF1 is a novel target gene of the p53 family and regulates cancer cell migration and invasiveness. Oncogene *33*, 4837–4846.

Thiel, A.T., Blessington, P., Zou, T., Feather, D., Wu, X., Yan, J., Zhang, H., Liu, Z., Ernst, P., Koretzky, G.A., and Hua, X. (2010). MLL-AF9-induced leukemogenesis requires coexpression of the wild-type Mll allele. Cancer Cell *17*, 148–159.

van der Flier, L.G., van Gijn, M.E., Hatzis, P., Kujala, P., Haegebarth, A., Stange, D.E., Begthel, H., van den Born, M., Guryev, V., Oving, I., et al. (2009). Transcription factor achaete scute-like 2 controls intestinal stem cell fate. Cell *136*, 903–912.

Wang, P., Lin, C., Smith, E.R., Guo, H., Sanderson, B.W., Wu, M., Gogol, M., Alexander, T., Seidel, C., Wiedemann, L.M., et al. (2009). Global analysis of H3K4 methylation defines MLL family member targets and points to a role for MLL1-mediated H3K4 methylation in the regulation of transcriptional initiation by RNA polymerase II. Mol. Cell. Biol. *29*, 6074–6085.

Warrier, S., Bhuvanalakshmi, G., Arfuso, F., Rajan, G., Millward, M., and Dharmarajan, A. (2014). Cancer stem-like cells from head and neck cancers are chemosensitized by the Wnt antagonist, sFRP4, by inducing apoptosis, decreasing stemness, drug resistance and epithelial to mesenchymal transition. Cancer Gene Ther. *21*, 381–388.

Welkoborsky, H.J., Jacob, R., Riazimand, S.H., Bernauer, H.S., and Mann, W.J. (2003). Molecular biologic characteristics of seven new cell lines of squamous cell carcinomas of the head and neck and comparison to fresh tumor tissue. Oncology *65*, 60–71.

Wend, P., Fang, L., Zhu, Q., Schipper, J.H., Loddenkemper, C., Kosel, F., Brinkmann, V., Eckert, K., Hindersin, S., Holland, J.D., et al. (2013). Wnt/β-catenin signalling induces MLL to create epigenetic changes in salivary gland tumours. EMBO J. *32*, 1977–1989.

Winters, A.C., and Bernt, K.M. (2017). MLL-rearranged leukemias—an update on science and clinical approaches. Front Pediatr. *5*, 4.

Wolf, J.S., Chen, Z., Dong, G., Sunwoo, J.B., Bancroft, C.C., Capo, D.E., Yeh, N.T., Mukaida, N., and Van Waes, C. (2001). IL (interleukin)-1alpha promotes nuclear factor-kappaB and AP-1-induced IL-8 expression, cell survival, and proliferation in head and neck squamous cell carcinomas. Clin. Cancer Res. *7*, 1812–1820.

Wong, S.H., Goode, D.L., Iwasaki, M., Wei, M.C., Kuo, H.P., Zhu, L., Schneidawind, D., Duque-Afonso, J., Weng, Z., and Cleary, M.L. (2015). The H3K4-methyl epigenome regulates leukemia stem cell oncogenic potential. Cancer Cell *28*, 198–209.

Ying, Y.L., Johnson, J.T., and Myers, E.N. (2006). Squamous cell carcinoma of the parotid gland. Head Neck *28*, 626–632.

Yokoyama, A., Somervaille, T.C., Smith, K.S., Rozenblatt-Rosen, O., Meyerson, M., and Cleary, M.L. (2005). The menin tumor suppressor protein is an essential oncogenic cofactor for MLL-associated leukemogenesis. Cell *123*, 207–218.

Zhang, L., Xia, Y., Li, L., Wang, Y., Liu, Y., Li, C., and Yu, T. (2012). Cancer stem cell-like cells exist in mucoepidermoid carcinoma cell line MC3. Oncol. Res. *20*, 589–600.

Zhu, J., Sammons, M.A., Donahue, G., Dou, Z., Vedadi, M., Getlik, M., Barsyte-Lovejoy, D., Al-awar, R., Katona, B.W., Shilatifard, A., et al. (2015). Gain-of-function p53 mutants co-opt chromatin pathways to drive cancer growth. Nature *525*, 206–211.

Zoncu, R., Efeyan, A., and Sabatini, D.M. (2011). mTOR: from growth signal integration to cancer, diabetes and ageing. Nat. Rev. Mol. Cell Biol. *12*, 21–35.

STAR★METHODS

KEY RESOURCES TABLE

REAGENT or RESOURCE	SOURCE	IDENTIFIER
Antibodies		
Rabbit polyclonal anti-H3K4me1	Diagenode	Cat#C15410194; RRID:AB_2637078
Rabbit polyclonal anti-H3K4me2	Diagenode	Cat#C15410035
Rabbit polyclonal anti-H3K4me3	Diagenode	Cat#pAb-003-050; RRID:AB_2616052
Rabbit polyclonal anti- Histone H3	Abcam	Cat#ab1791; RRID:AB_302613
Mouse monoclonal anti-β-catenin	BD Bioscience	Cat#610153; RRID:AB_397554
Rabbit monoclonal anti-Lef1	Cell Signaling Technology	Cat#2230; RRID:AB_823558
Rabbit monoclonal anti-Tcf4	Cell Signaling Technology	Cat#2569; RRID:AB_2199816
Rabbit polyclonal anti-Axin2	Cell Signaling Technology	Cat#2151; RRID:AB_2062432
Mouse monoclonal anti-E-cadherin	BD Bioscience	Cat#610181; RRID:AB_397580
Rabbit polyclonal anti-Tri-Methyl-Histone H3(Lys4)	Cell Signaling Technology	Cat#9727; RRID:AB_561095
Rabbit polyclonal anti-Tri-methyl histone H3 (Lys27)	Millipore	Cat#07-449; RRID:AB_310624
Rabbit polyclonal anti-H3	Abcam	Cat#ab1791; RRID:AB_302613
Rabbit polyclonal anti-Mll1	Bethyl	Cat#A300-086A; RRID:AB_242510
Rabbit polyclonal anti-Mll1	Bethyl	Cat#A300-374A; RRID:AB_345243
Rabbit polyclonal anti-CBP(A22)	Santa Cruz Biotechnology	Cat#sc-369; RRID:AB_631006
Mouse monoclonal anti-α-Tubulin	Sigma Aldrich	Cat#T9026; RRID:AB_477593
Guinea pig polyclonal anti-Cytokeratin 8	ARP American Research Products	Cat#03-GP-K8; RRID:AB_1541063
Mouse monoclonal anti-Cytokeratin 14	Thermo Fisher Scientific	Cat#MA5-11599; RRID:AB_10982092
Rabbit polyclonal anti-Cleaved caspase-3	Cell Signaling Technology	Cat#9661; RRID:AB_2341188
Rabbit monoclonal anti-Ki67	Lab Vision	Cat#RM-9106; RRID:AB_2335745
Chemicals, Peptides, and Recombinant Proteins		
ICG-001	Selleckchem	S2662
LF3	Chemdiv	5743-0262
MI-2	Selleckchem	S7618
JQ1	Toris	4499
C646	Sigma	SML002
I-CBP112	Sigma	SML1134
FGFb	Thermofisher	PGH0021
EGF	Life technologies	PHG0313
Insulin	Sigma-Aldrich	91077C
Dexamethasone	Sigma-Aldrich	Dexamethasone
Wnt3a	R&D	1324-WN
Y-27632	Selleckchem	S1049
Tryplex	GIBCO	12563
Matrigel	Corning	356231
Critical Commercial Assays		
iDeal ChIP-seq kit for Histone	Diagenode	C01010051
iDeal Library Preparation Kit	Diagenode	C05010020
TruSeq stranded mRNA library preparation kit	Illumina	20020594
TruSeq SBS Kit v3-HS	Illumina	FC-401-3001
GeneChip 3′IVT express kit	Applied Biosystems	902416

(Continued on next page)

Continued

REAGENT or RESOURCE	SOURCE	IDENTIFIER
Deposited Data		
RNA-seq data	This paper	GEO: E-MTAB-7509
Microarray data, see Table S6	This paper	N/A
Chip-seq data	This paper	GEO: E-MTAB-7514
Experimental Models: Organisms/Strains		
C57BL/6J mouse strain	Jackson Labs	000664
Mouse B6: *K14-Cre(Δneo)*	Wend et al., 2013	N/A
Mouse B6: *β-catenin^flox*	Wend et al., 2013	N/A
Mouse B6: *Bmpr1a^flox*	Wend et al., 2013	N/A
Mouse B6: *Mll1^flox*	Chen et al., 2017	N/A
Mouse B6: *K14-Cre; Bmpr1a^{flox/+}; Mll1^{flox/+}*	This study	N/A
Mouse B6: *β-catenin^{flox/flox}; Bmpr1a^{flox/flox}; Mll1^{flox/flox}*	This study	N/A
Mouse B6: *K14-Cre; β-catenin^{flox/+} Bmpr1a^{flox/flox}; Mll1^{flox/flox}*	This study	N/A
Oligonucleotides		
sgRNAs used for gene deletion, see Table S1	This study	N/A
sgRNAs used for Mll1 domain mutagenesis, see Table S2	This study	N/A
Primers for RT-qPCR and ChIP-qPCR, see Table S5	This study	N/A
PCR Primers Used to Amplify Mll1 Mutant Regions for Next Generation Sequencing Analysis, see Table S7	This study	N/A
Software and Algorithms		
Flowjo	FLOWJO LLC	N/A
R	R-studio	N/A
STAR	Dobin et al., 2013	N/A
DESeq2	Hashimshony et al., 2016	RRID:SCR_015687; https://genomebiology.biomedcentral.com/articles/10.1186/s13059-014-0550-8
CRISPResso	Pinello et al., 2016	http://crispresso.rocks/

CONTACT FOR REAGENT AND RESOURCE SHARING

Further information and requests for resources and reagents should be directed to and will be fulfilled by the Lead Contact, Walter Birchmeier (wbirch@mdc-berlin.de).

EXPERIMENTAL MODEL AND SUBJECT DETAILS

Cell culture

In sphere culture, 24-well cell culture plates were pre-coated with 250 μL poly-hydroxyethyl-methacrylate (PolyHEMA, 12 mg/ml in 95% ethanol, Sigma). Cells were seeded as single cells in sphere culture medium (F12:DMEM 1:1, containing 1X B-27 supplement, 20 ng/ml EGF, 20 ng/ml FGF, 5 μg/ml insulin and 0.5% methylcellulose). For obtaining adherent cells, mouse salivary gland tumor cells were cultured in DMEM/F12 medium supplemented with 20% knockout serum replacement (KSR), non-essential minimal amino acids, penicillin/streptomycin solution, L-glutamine and β-mercaptoethanol (Invitrogen). Human head and neck carcinoma cell lines were cultured in DMEM/F12 medium supplemented with 10% fetal bovine serum, penicillin and streptomycin. For self-renewal assay, cells were treated and let to form spheres. Primary spheres were dissociated and plated in plates at 4 cell per microliter dilutions. MI-2 (3.125 μM) and DMSO treatments were performed for 7 days. After treatment, spheres were dissociated, counted, and plated for self-renewal assay with the drugs. After 1 week, spheres were counted.

Mice

K14-Cre(Δneo), β-catenin^flox, Bmpr1a^flox, and *Mll1^flox* mice and the Cre-inducible *R26^EYFP* reporter allele have been described (Harada et al., 1999; Huelsken et al., 2001; Kranz et al., 2010; Mishina et al., 2002; Srinivas et al., 2001). All mice used in this study had a C57BL/6 background. The conditional gain-of-function mutation of β-catenin was produced by crossing homozygous mice carrying the *β-catenin^{lox(ex3)}* allele to *K14-cre* mice. The loss-of-function mutation of the *Bmpr1a* was produced by crossing

homozygous mice carrying *Bmpr1a^flox* alleles to *K14-cre* mice that were homozygous for the *Bmpr1a^flox* allele (Wend's paper). To obtain *Mll1* single mutant mice, male mice carrying *K14-Cre; Mll1^f/+* were crossed with female mice carrying *Mll1^f/+; R26^EYFP/EYFP*. Due to the infertility of *K14-Cre; β-catenin^flox/+* mice, in order to obtain triple mutant mice, we first generated *K14-Cre; Bmpr1a^flox/+; Mll1^flox/+* mice and *β-catenin^flox/flox; Bmpr1a^flox/flox; Mll1^flox/flox* mice. Both these two mouse strains were fertile and showed no aberrant phenotype. To generate *K14-Cre; β-catenin^flox/+ Bmpr1a^flox/flox; Mll1^flox/flox ; ROSA26^EYFP/+*, we always crossed male *K14-Cre; Bmpr1a^flox/+; Mll1^flox/+* with female *β-catenin^flox/flox; Bmpr1a^flox/flox; Mll1^flox/flox ; ROSA26^EYFP/+*. Mutant mice were genotyped by PCR. Animal experiments were performed according to the EU and national institutional regulations.

METHOD DETAILS

ChIP-Seq and mRNA-seq

Anti-H3K4me1 (C15410194), -me2 (C15410035) and -me3 (C15410003-50) antibodies were purchased from Diagenode. ChIP-seq was performed according to the protocols provided by Diagenode using the iDeal ChIP-seq kit for histones and the iDeal library preparation kit. For mRNA-seq, mRNA was extracted according to the standard TRIzol protocol (Invitrogen) and subjected to library preparation using the TruSeq stranded mRNA library preparation kit. Sequencing was performed with the TruSeq SBS Kit v3-HS (2 X 200 cycles) on an Illumina HiSeq 2000 sequencer.

Compounds

ICG-001 (25 μM; S2662, Selleckchem), LF3 (50 μM; 5743-0262, Chemdiv), MI-2 (50 μM; S7618, Selleckchem), JQ1 (25 μM; 4499, Toris), C646 (25 μM; SML0002, Sigma) and I-CBP112 (25 μM; SML1134, Sigma) were prepared as concentrated stock solutions in DMSO, and were diluted in culture medium to obtain the final concentrations. The final concentrations of DMSO were kept equal for all treatments.

CRISPR/Cas-based Gene Deletion and Domain Mutagenesis

pSpCas9(BB)-2A-GFP (PX458) was a generous gift from Feng Zhang (Addgene plasmid # 48138). The PX458-mCherry plasmid was generated by replacing the GFP cassette in PX458 with mCherry. sgRNAs were designed on https://zlab.bio/guide-design-resources and inserted into PX458-mCherry according to the protocol described (Ran et al., 2013). Target cells were transfected with constructed PX458-mCherry plasmids using Lipofectamine 2000. 48 h after transfection, mCherry⁺ cells were FAC-sorted for analyzing gene deletion deficiency or generating mutant cell clones. sgRNAs used for *Mll1* deletion are listed in Table S1. The pT2-HB-Cas9-2A-mCherry plasmid was generated by inserting the Cas9-2A-mCherry expression cassette into pT2-HB plasmid. pT2-HB-Cas9-2A-mCherry and pCMV(CAT)T7-SB100 were co-transfected into target cells. After one week, stable mCherry-expressing cells were FAC-sorted and mixed with parental cells at 4:1 ratios. sgRNAs targeting different domains of Mll1 were designed on https://zlab.bio/guide-design-resources and inserted into the lentiGuide-Puro vector. Viral particles expressing sgRNAs were produced and used to transduce target cells according to the described protocol (Sanjana et al., 2014). After Puromycin selection, cells were subjected to sphere culture, and FACS was used to analyze the mCherry⁺ cells. sgRNAs used for Mll1 domain mutagenesis are listed in Table S2.

Immunofluorescence and other Stainings

Immunofluorescence and H&E staining were performed on formalin-fixed paraffin-embedded tissue sections as we had described (Huelsken et al., 2001). Antigen retrieval was accomplished by Tris-EDTA (10 mM Tris, 1 mM EDTA, 0.05% Tween-20, pH 9.0) at 99-100°C for 20 minutes. Following retrieval, sections were stained by Hematoxylin-Eosin (HE) or different antibodies. The following primary antibodies were used for immune-detection: mouse anti-β-catenin (from BD Transduction Laboratories), rabbit anti-trimethyl histone H3K4me3 and rabbit anti-tri-methyl histone H3K27me3 (Cell signaling), guinea pig anti-CK8, mouse anti-CK10 and rabbit anti-CK14 antibodies (Covance). Images were captured using an Axio imager.Z1m and AxioCam MRm (Carl Zeiss).

Quantitative Real-Time PCR

After desired treatments, cells were lysed in suitable amounts of TRIzol (Invitrogen), and 2 μg total RNA was reverse-transcribed using MMLV reverse transcriptase (Promega) according to the instructions by the manufacturers. qRT-PCR was performed using the iCycler IQTM 5 multicolor real-time detection system (Bio-Rad) with absolute SYBR green fluorescein (ABgene). PCR was carried out following a standard protocol: primer sequences used for qRT-PCR can be found in Table S5.

Immunoprecipitation and Western Blotting

For immunoprecipitation, cells were lysed in Co-IP buffer containing 50 mM Tris pH7.5, 150 mM NaCl, 1% NP-40, 10% Glycerol, 1 mM DTT, 1 mM PMSF, and protease inhibitor cocktail (Roche). 500 μg of total protein extract for each sample was pre-cleaned by protein G Dynabeads (Thermo Fisher) at 4°C for 1 h. Pre-cleaned lysate was sequentially incubated with anti-β-catenin (610154, BD Transduction Laboratories), anti-Lef1 (2230, Cell signaling) and anti-Tcf4 antibodies (2953, Cell signaling) at 4°C overnight and subsequently with protein G Dynabeads for an additional 1 h. All washing and incubation steps were carried out in Co-IP buffer. The bound proteins were eluted by boiling in SDS sample buffer and analyzed by western blotting.

Protein samples from different experiments were loaded onto 8%–12% SDS-PAGE, separated in the electrophoresis running buffer (25 mM Tris, 20mM glycine, 2% SDS), and transferred onto PVDF membranes in the transfer buffer (25 mM Tris, 192 mM glycine, 3% SDS, 10% methanol). Non-specific binding sites on the membranes were blocked for 1 h at room temperature (RT) in blocking solution (4% BSA, 0.1% Tween20 in PBS) with constant shaking. The primary antibodies were diluted in blocking solution and incubated with the membranes at 4°C overnight with constant shaking. After washing in PBST (0.1% Tween20 in PBS), the membranes were incubated with the HRP-conjugated secondary antibodies diluted in blocking solution for 1 h. After washing three-times in PBST, the immuno-reactive bands were visualized with Western lightning chemi-luminescence reagent plus (PerkinElmer) and a Vilber Lourmat imaging system SL-3. The following primary antibodies were used for immune-detection: mouse anti-β-catenin (from BD Transduction Laboratories), rabbit anti-β-catenin (Huelsken et al., 2001), rabbit anti-Axin2 and rabbit anti-tri-methyl histone H3 (Lys4) (Cell Signaling), rabbit anti-tri-methyl histone H3 (Lys27) (Millipore), rabbit anti-Mll1 (Bethyl), mouse anti-TCF4 antibody (Cell Signaling), mouse anti-E-cadherin (BD Transduction Laboratories), rabbit anti-CBP and mouse anti-α-tubulin antibodies (Sigma).

Organoid Culture

Mouse salivary organoid cultures were generated and maintained as described in a protocol that we adapted (Maimets et al., 2016). Briefly, murine salivary glands of mice with different genotypes were dissected and enzymatically digested with collagenase type II (GIBCO) and Dispase. Cell aggregates were embedded directly in growth factor-reduced Matrigel (Corning). Cells with K14-Cre activity bearing the EYFP-reporter were FACS-enriched before seeding. Matrigel was overlaid in a 1:10 ratio with Salivary gland medium (SGM) composed of DMEM/F12 medium supplemented with B27 and N2, 10 mM HEPES, Glutamax, Penicillin/Streptomycin (all from Life technologies), 1.25 mM N-acetylcysteine (N-AC, Sigma-Aldrich), and the following growth factors: 50 ng/ml EGF (Life technologies), 20 ng/ml FGFb (GIBCO), 10μg/ml insulin (Sigma-Aldrich) and 1μM dexamethasone (Sigma-Aldrich). After FACS-enrichment, cells were cultured for 1 day in the presence of the 10μM Rock inhibitor Y-27632 (Selleck Chemical). Organoids were passaged by cell dissociation using TrypLEX (GIBCO). For retrovirus infection, salivary gland organoids were dissociated by TrypLEX (GIBCO) and transferred to SGM enriched with 500ng/ml Wnt3a (R&D), 5mM Nicotinamide (Sigma), 10μM Rock inhibitor Y-27632, 8μg/ml Polybrene and the Cre-expressing virus (produced in Phönix cells). After Spin occulation, cells were cultured for 6h under non-adherent conditions in a cell culture incubator, before embedding into Matrigel and further cultured in SGM. For compound treatment, salivary gland organoids were cultured in SGM supplemented with the indicated concentrations of MI-2, with medium changes every second day for up to 4 days.

Cell Cycle and Apoptosis Analyses

Fresh cells were incubated with 5 μg/ml propidium iodide (Sigma) in PBS for 10 min and analyzed for cell death using FACS (BD Transduction Laboratories). For apoptosis analyses, cells fixed with 3% formaldehyde were sequentially incubated with anti-cleaved-caspase3 antibody (9661, Cell signaling) and DyLight488-conjugated secondary antibody (711-485-152, Jackson ImmunoResearch laboratories) in PBS with 0.5% BSA. The percentage of cleaved-caspase3-positive cells was analyzed by the FACS (BD Transduction Laboratories).

Xenotransplantation Studies

Cells with different genotypes (5000 or 500 cells) were subcutaneously injected into the back skin of NOD-SCID mice, 3 per group. Tumor growth was monitored over a period of 100 days.

Gene Expression Profiling by Microarray

Total RNA of HNSCCUM-03T cells was extracted according to the standard TRIzol protocol (Invitrogen), and prepared with GeneChip 3′IVT express kit (Illumina) for the microarray analysis using Microarray U133A 2.0. Microarray data were processed and analyzed with R Studio to find differentially regulated genes. Most differentially-regulated genes were subjected to gene set enrichment analysis. Different gene sets were downloaded from http://software.broadinstitute.org/gsea/index.jsp. Microarray gene expression data can be found in Table S6.

ChIP-seq and mRNA-seq Data Analysis

All sequencing reads were mapped using STAR (v 2.5.3a) with the parameter "-alignIntronMax 1" with the purpose of disable splicing alignments. Peak detection was performed by MACS2 (default parameter for narrow peak detection) on bam files on each sample. We created a unique reference peak file for each histone modification by merging all individual peak files. FeatureCounts software was used for counting reads on each sample for the corresponding reference peak file. Significant (adjusted p value < 0.01) differential peak enrichments were identified by DESeq2. Peaks with low read counts (baseMean < 50) and small difference of enrichment (log2FC < 0.6 or log2FC > −0.6) were discarded. The generation of Wig files for plotting the genome tracks was done by the Bioconductor package MEDIPS. A sliding window of 50bp was used to plot high resolution normalized fpkm values in the whole genome. ChIP-seq peak-calling data and mRNA-seq differential-expression data can be found in Tables S3 and S4.

Mutation Abundance Measurement by NGS

To analyze the mutation abundance of target regions, primary PCR was used to amplify mutant regions, and secondary PCR was performed to add adaptors for next generation sequencing. PCR primers for these procedures are listed in Table S7. The quantification of CRISPR genome editing outcomes were obtained using command line version of CRISPResso tool (http://crispresso.rocks/). Indels were then assigned as Frameshift deletions (FS) and In-frame deletions (IF). FS were assigned, when the number of deleted was not a multiple of three and IF, when the number of deleted was a multiple of three. Finally, reads of 50 most abundant mutations (FS and IF) were added up, and the proportion of FS and IF was compared among the different time points.

QUANTIFICATION AND STATISTICAL ANALYSIS

All data shown are presented as mean ± SEM, all the statistical details of experiments can be found in the figure legends. When comparing datasets, two-tailed unpaired Student's t test was applied using GraphPad Prism software, unless indicated. No statistical method was used to estimate the sample size. No specific randomization or blinding protocol was used. N indicates the numbers of independent biological replicas per experiment unless otherwise indicated. $p \leq 0.05$ was considered statistically significant. Significance tests were performed on all samples and therefore graphs lacking p values indicate results were not statistically significant.

DATA AND SOFTWARE AVAILABILITY

The accession numbers for the ChIP-seq and RNA-seq data reported in this paper can be found under Gene Expression Omnibus GEO: E-MTAB-7514 and E-MTAB-7509, respectively.